International Journal of Refrigeration 137 (2022) 188–211

Contents lists available at ScienceDirect

International Journal of Refrigeration

journal homepage: www.elsevier.com/locate/ijrefrig

Modelling and Analysis of Ammonia Sorption Reactions in Halide Salts

Modélisation et analyse des réactions de sorption de l'ammoniac dans les halogénures

S. Hinmers [a,*], G.H. Atkinson [a], R.E. Critoph [a], M. van der Pal [b]

[a] School of Engineering, University of Warwick, Coventry, CV4 7AL, UK
[b] TNO Energy Transition, Westerduinweg 3, 1755LE Petten, The Netherlands

ARTICLE INFO

Keywords:
Chemisorption
Ammonia
Halide salts
Composite matrix
Experimental
Modelling

Mots clés:
Chimisorption
Ammoniac
Halogénures
Matrice composite
Expérimentation
Modèlisation

ABSTRACT

This work has focussed on the development of an accurate method for testing and modelling the reaction kinetics involved in ammonia-salt adsorption reactions, something not achieved consistently to date. A Large Temperature Jump (LTJ) test cell has been developed for testing ammonia-salt reactions in real machine conditions. A Large Temperature Jump (LTJ) test cell has been developed for testing ammonia-salt reactions in real machine conditions. This was used to validate a new approach to modelling the behaviour and simulate the performance of chemisorption machines. A derivation of the heat transfer and thermodynamic equations are presented, and a finite difference model described which has been validated for the adsorption and desorption reactions of ammonia into halide salts within a porous matrix. The model is implemented in a MATLAB® program. Large Temperature Jump (LTJ) tests have been conducted on manganese chloride and barium chloride to validate the model and to identify the physical parameters which characterise the dynamic performance of the sorbent. The manganese chloride and barium chloride were impregnated in expanded natural graphite (ENG) (SGL SIGRATHERM®) board. The ENG board gave rise to practicable samples (31.5 mm OD ø over ½" tube) undergoing a desorption reaction in under 250 seconds with the fluid temperature 15°C above the equilibrium temperature, an order of magnitude faster than observed elsewhere. A new test method has been developed enabling an accurate single heat of reaction to be identified due to reduced hysteresis, which is reported for barium and manganese chloride. The model has been validated using experimental data from LTJ tests of two geometric configurations in radial heat transfer: discs heated/cooled from the outside radius ('tube-side') and annuli heated from the inner radius ('shell-side'). The empirical data obtained is a milestone towards designed and optimised salt generators.

1. Introduction

The chemisorption of ammonia into halide salts has been studied over many years: it was first observed by Faraday who recognised its potential for generating a heating or cooling effect (Faraday, 1823); more recently it garnered attention in the '80s and '90s, primarily by Spinner (Spinner, 1988), and many others (Goetz et al., 1993; Lebrun and Spinner, 1990b; Mazet and Spinner, 1994). There has been a resurgence in contemporary interest such as by Zhou et al. (Zhou et al., 2016), and Sharonov and Aristov due to its potential to decarbonise heating (Sharonov and Aristov, 2005). Cycles using chemisorption can be applied to refrigeration, heat pumping, and thermal transformation and may either use a single salt in a reactor together with a system for evaporating and condensing the refrigerant, or a resorption cycle in which the refrigerant is adsorbed or desorbed between two salts. More complex three salt cycles with varying degrees of complexity and heat recovery are also possible, as illustrated by An et al. (An et al., 2019).

The most recent review on ammonia-based chemisorption reactions for heat pumping is by Yang et al. (Yang et al., 2020). One of the main conclusions related to the material-salt combination is that the "*hysteresis of sorbent salts […] can significantly affect the performance or even viability of the chemisorption system.*" The work reported here, which is mainly concerned with two-salt resorption cycles for heat pumping and thermal transformation applications, aims to prove that with careful salt-pairing selection (for the High Temperature Salt (HTS) and Low Temperature Salt (LTS)), coupled with an inherent understanding of the hysteresis phenomena and the final-use application, the dynamic performance of halide-salts can be predicted and utilised effectively for prototype systems.

* Corresponding author.
E-mail address: s.hinmers@warwick.ac.uk (S. Hinmers).

https://doi.org/10.1016/j.ijrefrig.2022.01.032
Received 23 September 2021; Received in revised form 28 January 2022; Accepted 31 January 2022
Available online 2 February 2022

Nomenclature

A_r	Arrhenius constant in rate equation
c_V	Specific heat at constant volume (J kg^{-1} K^{-1})
dm	Increment of mass (kg)
h	Specific enthalpy (J kg^{-1})
MC_p	Heat capacity- comprised of ENG and salt fixed masses (J K^{-1})
m	mass (kg)
n	Constant in reaction rate equation (-)
p	Pressure (Pa)
Q	Heat (J)
R	Gas constant (J kg^{-1} K^{-1})
s	Specific entropy (J kg^{-1} K^{-1})
t	Time (s)
U	Internal Energy (J)
T	Temperature (K)
u	Specific Internal Energy (J/kg)
v	Specific volume (m^3 kg^{-1})
V	Volume (m^3)
X	Degree of 1st reaction 0 to 1 (mol/mol)
Y	Degree of 2nd reaction 0 to 1 (mol/mol)

Greek

Δh	Change in enthalpy (J kg^{-1})
ΔQ	Heat entering system (J)
Δs	Change in entropy (J kg^{-1} K^{-1})
ΔU	Change in internal energy (J)

Subscripts

A	Pertaining to type A adsorbate with .A mols of ammonia
AB	Reaction from type A to type B
ADS	Adsorbate
ads	Adsorption process
B	Pertaining to type B adsorbate with .B mols of ammonia
BC	Reaction from type B to type C
C	Pertaining to type C adsorbate with .C mols of ammonia
des	Desorption process
E	Expansion vessel
ENG	Expanded Natural Graphite
eq	Equilibrium
GAS	Gas
HYS	Hysteresis
in	Inlet
NR	Non-reacting portion
out	Outlet
PROD	Product
R	Reacting portion
REACT	Reactant
SALT	Salt
V	Void

In the past, the major challenges to the development of chemisorption cycles have been attributed to: agglomeration; heat and mass transfer; and slow reaction rates. In this study the salts are impregnated into Expanded Natural Graphite (ENG) sheet (SIGRATHERM® Graphite Lightweight Board, ECOPHIT® L10/1500) in order to keep the crystals dispersed. This avoids agglomeration, improves heat transfer and has been validated experimentally by van der Pal and Critoph (van der Pal and Critoph, 2017). The measured sheet density is 196 kg m^{-3} and the thermal conductivity in the plane of the sheet is 26 W m^{-1} K^{-1} as obtained from the manufacturer's data sheets (SGL Carbon, 2020).

1.1. Experimental work in literature

The general approaches to ammonia-salt chemisorption applied research has focussed around two methods, typically a full scale reactor is built without reporting previous experimental work, or a design is produced based on gravimetric testing. The authors propose that the reason significant advances have not occurred in this field of chemisorption is due to the lack of accurate modelling for optimised designs; as well as key factors such as thermal masses of fluids being omitted from data, restricting incremental advances in design from subsequent research. The absence of thermal mass reporting is well discussed by Gluesenkamp et al. (Gluesenkamp et al., 2020).

When we consider the full scale reactor approach there are a number of examples. Van der Pal and Critoph focussed primarily on a calcium chloride adsorption reactor, as previously mentioned the material performed effectively but thermal masses need reducing in order to achieve a Coefficient of Performance (COP) of 0.35 (van der Pal and Critoph, 2017); Mazet et al. studied a reactor packed with 700 grams of calcium chloride and then derived a model based on their reactor results. The modelling is very interesting but the reaction times are in hours rather than minutes, which would limit specific power of any machine (Mazet et al., 1991). Lépinasse et al., built a resorption transformer and modelled it, but their COP calculation does not use dynamic data, therefore their COP of 0.33 may be optimistic (Lépinasse et al., 1994). This work was continued by Goetz et al. but the model appears to be limited and key performance data is absent (Goetz et al., 1997). Vasiliev et al. constructed a resorption heat pump and reported a theoretical COP of 1.2. This was calculated using non-dynamic data. Thermal mass can be derived from their design but a COP calculated from dynamic data is important in understanding true system performance and 1.2 is relatively low for a heat pump (Vasiliev et al., 2004). Wang et al. built a resorption transformer, and calculated a COP of 0.2, but the result excludes thermal mass of the heat transfer fluid since the reactors were placed in thermostatic baths (Wang et al., 2010). Li et al. tested a resorption refrigeration machine and also calculate a COP for performance without using dynamic data, presenting a range of values based on potential conversion of sorbate (Li et al., 2010). Subsequent work has continued considering different applications with added complexity but not addressed the challenges first reported by Lépinasse et al., (Bao et al., 2011; Lépinasse et al., 2001; Xu et al., 2011). This shows the concept is well proven but advances towards a prototype have not occurred.

The other approach considering gravimetric testing has shown an insight into some of the reaction behaviour, but models developed from it have proven unreliable (An et al., 2020b; Moundanga-Iniamy and Touzain, 1992; Trudel et al., 1999; Zhong et al., 2009). The flaw with gravimetric methods is that they do not measure material temperature (causing important effects to be missed), and employ slow cycles which are unlike those experienced in real systems. These missed effects have been observed by Large Temperature Jump (LTJ) testing, such as a metastate which can cause incorrect Clapeyron relationships to be observed (Atkinson et al., 2021; Hinmers and Critoph, 2019). This leads to calculation error if heat of reaction values are derived from the Clapeyron relationships. The LTJ method is one of the best experimental methods developed to investigate the combination of heat and mass transfer and reaction rates, and was devised by Aristov et al. (Aristov et al., 2008). In the LTJ method a small sample of sorbent within a reactor is connected to a large gas reservoir and rapidly heated or cooled, desorbing or adsorbing refrigerant. The reservoir pressure is slightly but measurably altered. The change in pressure allows the rate of adsorption or desorption to be measured. In addition to being a simple

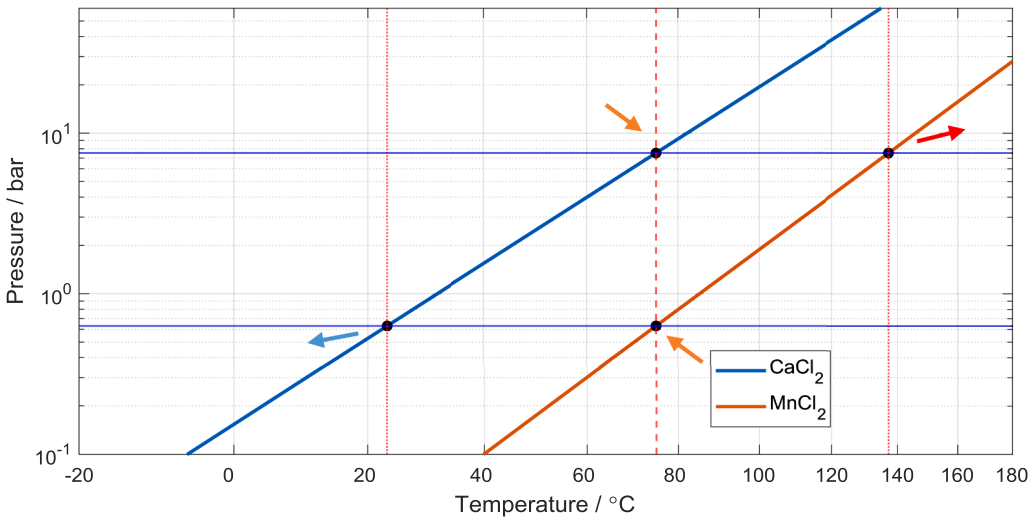

Fig. 1. Clapeyron diagram for a pairing of salts for a type (II) adsorption heat pump using equilibrium data from Neveu and Castaing (Neveu and Castaing, 1993). The waste heat is provided at both points illustrated with the orange arrows pointing into the apexes of the parallelogram, the recoverable waste heat is denoted by the red arrow aimed away, and heat lost to sink is denoted by the blue arrow furthest left.

technique, there is the advantage that the nominally constant pressure is similar to conditions experienced in a full-size machine.

1.2. Modelling work in literature

Recent modelling has taken the approach of fitting data to simple decaying exponential curves, for which a time constant is derived and used empirically to extrapolate to larger scales (Veselovskaya and Tokarev, 2011; Zhong et al., 2007). The motivation of this work was to determine physical parameters to describe the phenomena that occur during the reaction. Attempts to do this in the past have usually focused on an empirical model, but the results tend to produce different constants under different conditions. For example, one of the first approaches to use a theoretical model to dimension a working system was by Lebrun and Spinner, but in their validation, different packing densities and proportions of binders produce varying results (Lebrun, 1990; Lebrun and Spinner, 1990a, b). An improved approach was taken by Mazet et al., in which they separate the heat transfer and reaction model (Mazet et al., 1991) and in more contemporary work, similar approaches have been taken considering different analogical models. An et al. observed that a linear kinetic function (akin to the kinetic equation component presented by Mazet et al.) was reasonably effective at representing the reaction model for their tests with salts and ammonia. Their results however still suffered from deviation as great as ± 20% in some cases (An et al., 2020a).

The most effective model is the one which was developed by Mazet et al. (Mazet et al., 1991). Recent applications of it have returned mixed results: Jegede found an inconsistency in constants when modelling results (Jegede, 2017); whereas Hinmers and Critoph's results disprove this finding with unified constants when barium chloride reacted with ammonia (Hinmers and Critoph, 2019). A similar approach was taken by Atkinson et al. which also proved effective at predicting ammonium chloride and ammonia reactions with unified constants (Atkinson et al., 2021). This work builds on the model presented by Mazet et al., to produce an analogical model based on physical processes and to determine the physical parameters related to these reactions which is consistent and effective. With an accurate model, a basis is created for the reaction engineering of large-scale reactors, and an understanding of the challenges to designing ammonia-salt systems is developed. An effective model will inform the basis of optimised reactor designs and take resorption machines a step closer to realisation.

1.3. Resorption

Li et al compared the potential performance of resorption versus adsorption refrigeration systems using ammonia and salt, they illustrated that resorption systems have a higher maximum theoretical COP (Li et al., 2010). Furthermore, resorption systems lack evaporators and condensers, presenting the opportunity for cheap manufacture. For this reason, resorption appears to be a key application for ammonia-salt systems and is worthy of investigation. An obstacle to the development of resorption systems has been optimising system design as highlighted in section 1.1; to overcome this, it is important to produce a consistent and informative test method (such as using the LTJ method) and devising a model that can be used to optimise reactor design considering COP and power density.

To develop an understanding of the salts reacting with ammonia for resorption applications, barium chloride presents a simple case (reacting between 0 and 8 moles) to build an understanding of the process. The next salt to consider is manganese chloride as it is often paired with barium chloride and is a contender for a number of applications such as refrigeration, heat pumping, and heat transforming (type (II) heat pump), as proposed in the literature (Goetz et al., 1993; Li et al., 2010). To consider operation requirements, take the case of the type (II) heat pump. For this application, Goetz et al. propose the pairing of calcium chloride (8-4), with manganese chloride (6-2). To understand the operating requirements, a Clapeyron diagram can illustrate the operating temperatures. In this case the salts react at 75°C, to produce useful upgraded heat at a temperature in excess of 135°C. The upgraded heat is recovered, and some heat is rejected at a temperature of 24°C while the cycle resets. This is illustrated in Fig. 1 by plotting the Clapeyron lines from the data published by Neveu and Castaing (Neveu and Castaing, 1993). The details of the cycle process are explained by Goetz et al. (Goetz et al., 1993). This cycle shows a number of waste heat sources described as low grade can be used for thermal transformation. Waste heat sources such as steam condensate and other waste streams from cement, paper, and textiles industries are sourced at 90°C or above, as described by Ling-Chin et al. (Ling-Chin et al., 2019).

2. Methodology

2.1. Experimental Study - Large Temperature Jump Reactor (Tube side)

The sorption reactions of halide salts are observed using the LTJ

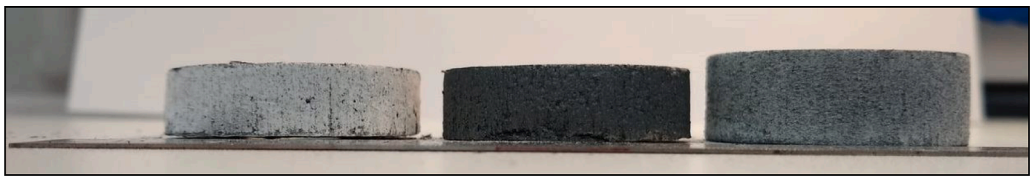

Fig. 2. Picture to illustrate the difference in swelling of samples once used. Left to right: a sample dosed with barium chloride with limited swelling; ENG without salt; and a manganese chloride sample that has increased slightly in outer diameter and height.

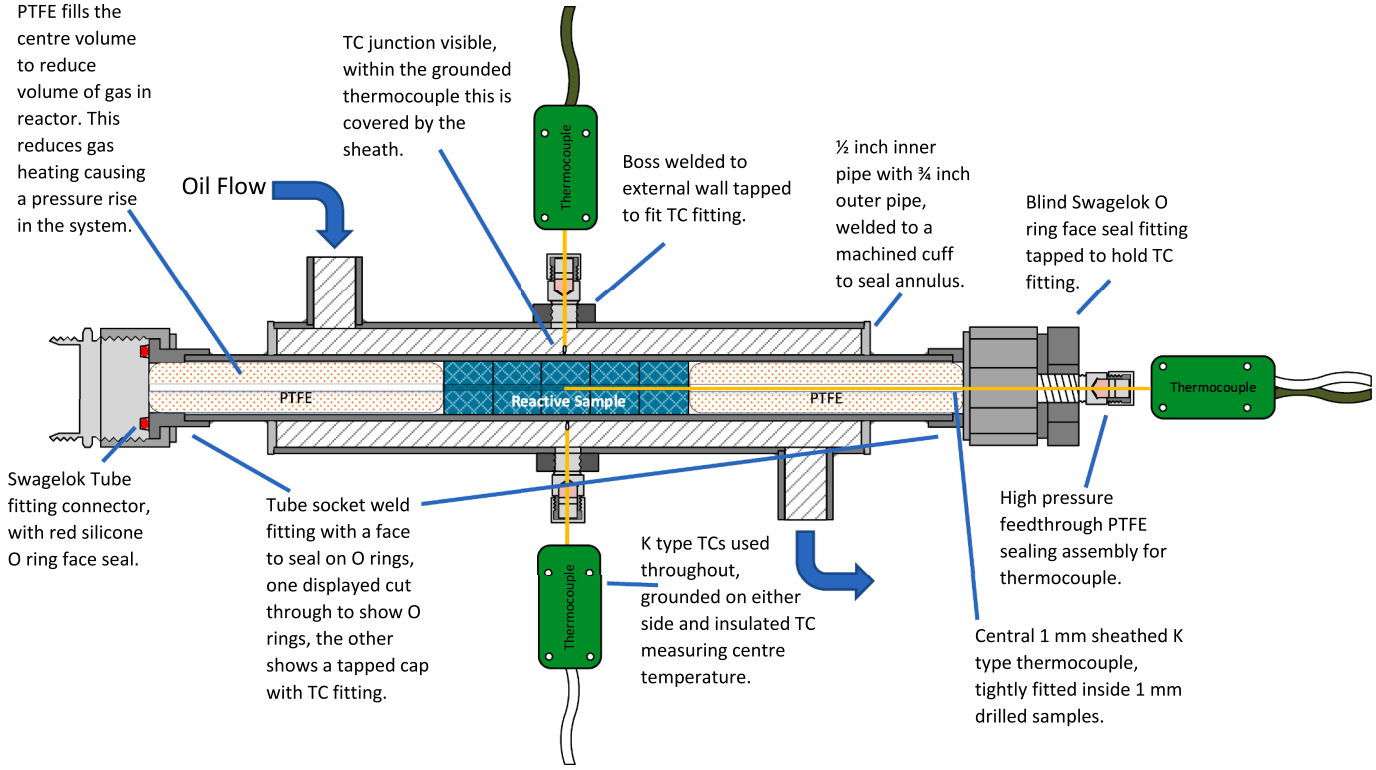

Fig. 3. Diagram detailing Large Temperature Jump (LTJ) tube-side reactor and components, note alternative terminals from thermocouples measuring wall temperature

technique. The method is applied as described by Hinmers and Critoph (Hinmers and Critoph, 2019). The LTJ uses a 'unit-cell' sorption reactor, which acts as a heat exchanger in contact with the adsorbent material. The reactor is heated and cooled with silicone oil (or water) from two temperature-controlled baths through a valve manifold, which isolates one of the baths while the other bath is connected to the reactor. When the baths are switched, the temperature of the oil flowing through the reactor 'jumps' up, or down, which initiates the sorption reaction. The reactor is connected to an expansion vessel, and the temperatures of the sorption material, reactor wall, and system pressure are measured at one second intervals.

2.1.1. *Experimental Method*

The design of Hinmers and Critoph (Hinmers and Critoph, 2019) has been modified. Previously, an insulated thermocouple (TC) measured the reactor wall temperature within the oil jacket, but it became clear that the reading was nearer to the oil temperature than the wall. The biased temperature reading was produced due to the thermal resistance between the TC and the wall, and thermal conduction to the large surface area of the TC sheath in the oil. To improve the wall temperature measurement, grounded TCs have been installed. By connecting one opposite polarity wire from each TC to diametrically opposite points on the tube wall, the TC junction becomes the reactor wall, rather than a welded tip immersed in heat transfer fluid at a slightly different temperature. Thus, the voltage reading from the thermocouple pair provides an average wall temperature at diametrically opposed points of the pipe. The modified configuration yields a more accurate reading for the wall temperature, which simplifies modelling of the LTJ.

An accurate measurement of the reactor wall temperature enables an accurate value for the rate of heat transfer between the sorption material and the stainless-steel wall to be identified, removing the need for also identifying a heat transfer coefficient for thermal oil to the stainless-steel wall, or for the temperature of the fluid to be known accurately. The conductivity of the stainless-steel (16 $Wm^{-1}K^{-1}$) and the graphite (26 $Wm^{-1}K^{-1}$ in the direction of heat conduction (SGL Carbon, 2020)) are both relatively large compared to thermal contact conductance between the two surfaces. This means the heat transfer resistance is dominated by the resistance between the reactor wall and composite. The heat transfer coefficient is quantified as an effective gas '*gap*' between the two materials across which heat is transferred by simple conduction. The '*gap*' or contact can vary between different salts since they swell by differing amounts within the material as shown in Fig. 2. The reactor design for the tube-side configuration can be seen in Fig. 3.

Additionally, the reactor was changed (compared with the design used by Hinmers and Critoph (Hinmers and Critoph, 2019)) by replacing the fittings connecting the reactor to the filling valves and expansion vessels (12 litres volume combined) with Swagelok O-ring face seal fittings. Using face seals made it easier to take the reactor apart between

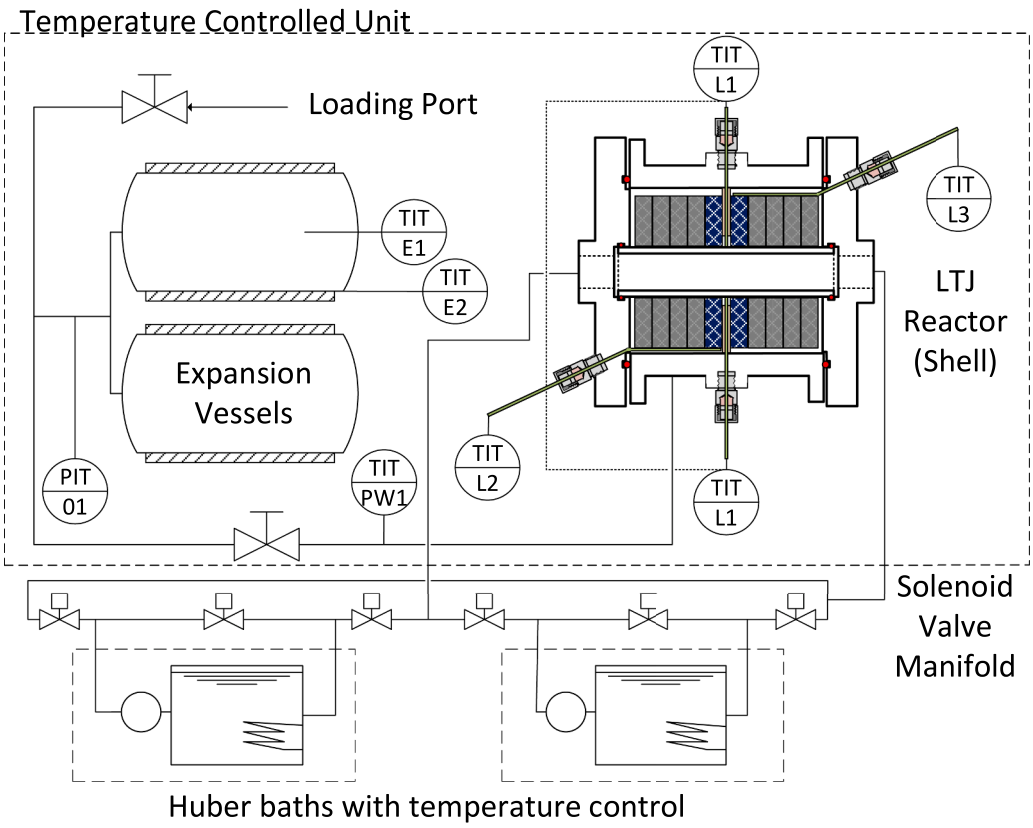

Fig. 4. Process Flow Diagram of LTJ Test Rig with shell-side LTJ reactor.

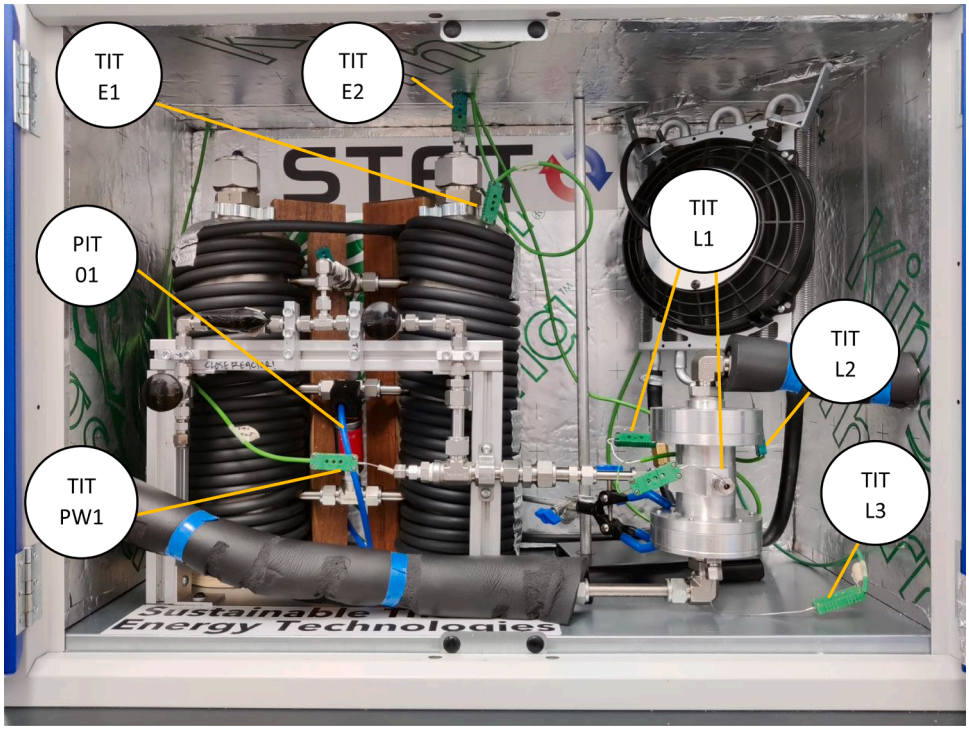

Fig. 5. LTJ rig with the shell-side reactor in the temperature-controlled cabinet. The reactor can be seen to be connected to the expansion vessels, via pipework with valves to isolate components. Insulated hoses feed silicone oil (or water) to the reactor. Labelled items correspond to those on Fig. 4. TIT L1 has two connections as it is the grounded thermocouple pair providing one reading as described.

Fig. 6. Grounded thermocouple contact with central pipe, a sample can be seen underneath.

tests and prevented deformation of connecting pipes from tightening of ferrule sealed tube fittings. The data acquisition device was also updated from an Omega DAQ to a NI CompactDAQ, with C series temperature and voltage input modules. The NI CompactDAQ reduced noise by separating the temperature and voltage signals. Separate modules and grounding wires prevented ground loops in the system or signals on the DAQ device. The pressure was measured with a Danfoss AKS 32 pressure transmitter, which was successfully calibrated with a deadweight pressure tester. The thermocouples were checked and operate within specified tolerance of 'typical accuracy', as detailed for the NI CompactDAQ C series thermocouple module at ±0.37°C. Details of both tests and results can be seen in the Research Data Link section.

2.1.2. Shell Side Reactor

To further evaluate the rigor of the model, a reactor that hosts the sorbent material in the shell (of a shell and tube heat exchanger) was designed, as shown in Fig. 5, Fig. 7 & Fig. 8. This is installed in place of the previous tube side LTJ reactor of Fig. 3. The shell-side reactor is formed of a central stainless-steel tube, through which the thermal oil flows (rather than the external annulus of the tube side reactor) and has an aluminium shell. The reactive samples fit tightly around the stainless-steel tube and the samples are isolated from the shell with a gas gap to reduce heat transfer. A two-millimetre ring of thermoplastic PEEK, (which was not in contact with the central tube as seen in Fig. 6) was used to direct the central thermocouples radial to the oil flow, allowing a measurement of the wall temperature. The guiding holes in the PEEK ring, were drilled at a slight angle to encourage the thermocouples to bend, creating a spring force ensuring contact on the pipe as shown in Fig. 6. In Fig. 7 it can be seen that ENG discs without salt were used to hold the sample in place and align the thermocouples. A previous iteration used PEEK cylinders with a gap to isolate from the central pipe (Appendix E). However, the thermoplastic had too much thermal mass and the thermocouple readings were less reliable, as shown in Appendix B, which presents the barium results in the shell. From the data in Appendix B, the thermocouples inserted axially measuring the outside of the sample were observed to drift from their expected readings, but the pressure rise in the system still provided a reasonable basis for measuring the rate of reaction and was predicted accurately by the model.

Similar, to the previous design, grounded thermocouples were used in contact with the centre pipe to provide a temperature reading of the pipe wall (Fig. 7, from the top and bottom). Sheathed thermocouples were fed through the tapped flange and aligned using the blank ENG to provide a temperature reading on the outer surface of the samples. The machined flanges and shell were sealed with silicone rubber O-rings (indicated in red in Fig. 7). A Swagelok fitting in the shell (seen in Fig. 8 on the right side) connects the reactor to the expansion vessels.

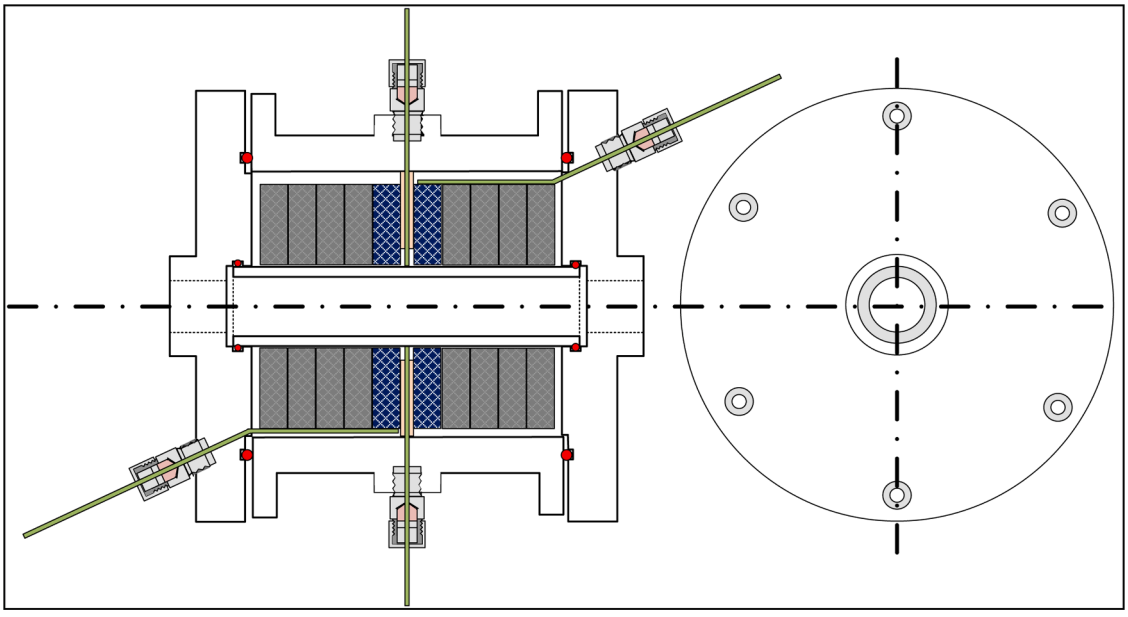

Fig. 7. Shell-side reactor design section. Positions of thermocouples can be seen in green. Red circles show O-rings in section. Samples dosed with salt appear blue (two central discs) whilst blank ENG appears grey (surrounding eight discs). A port connecting the reactor to the pipework as in Fig. 8 is perpendicular to the radial TC tapped fittings and cannot be seen in this diagram.

Fig. 8. Shell side reactor. The main shell is manufactured from a single piece of aluminium machined down to include bosses to mount TC fittings and a BSP fitting to connect to expansion vessels. The two flanges also made from the same piece of aluminium, the top and bottom are tapped with BSP Swagelok elbow connection and gasket seal. The end of the shell is sealed with large silicone O rings and the ½" central tube is sealed with two silicone O rings.

2.2. Sample Preparation

Manganese chloride and barium chloride were impregnated in ENG to form the reactive composite. For the tube side and shell side samples, discs of ENG were cut from the board (SIGRATHERM® Graphite Lightweight Board, ECOPHIT® L10/1500 (SGL Carbon, 2020)) with a water jet cutter. Tube side samples were cut (ø 10.8 mm discs) and then drilled with a 1 mm centre hole. Larger discs for the shell side were cut with an outer diameter of 34.5 mm on the waterjet cutter, and then a centre hole that fits tightly around a half inch tube was drilled with a custom hole saw. The samples' dimensions and specifications can be seen in Table 1. The discs were heated in an oven for an hour at 210 °C to remove any moisture before being weighed. To impregnate with salt, the samples were held submerged in beakers of prepared aqueous solution. The beakers were placed in a vacuum chamber and evacuated for 24 hours. The samples were then removed from the solution and dried in an oven at 210°C for another hour, before being weighed again to measure salt uptake.

The salt solutions were prepared near to saturation at room temperature, on a hot plate stirrer with warming and agitation. It is worth noting that the solvation of anhydrous manganese chloride is very exothermic and can result in an oxide forming which produces a brown opaque sediment within the liquid, rather than the desired translucent pink or clear solution. Solutions prepared with manganese chloride tetrahydrate were found to produce samples with mass uptake of salt and active fraction, similar to the other salts and no brown sediment or opacity was observed.

Once the salt uptake was measured, the samples were placed in the appropriate reactor (shell or tube side) and connected to the rig. The rig was then connected to a vacuum pump and evacuated for 2 hours while the reactor was heated to 60°C. Weighing was done quickly to minimise the time in which the samples may adsorb any moisture from the air.

3. Results

3.1. LTJ results

During an LTJ cycle the adsorption or desorption reaction was initiated by switching the temperature-controlled baths circulating silicone oil through the reactor. Once the pressure had stabilised, the baths were switched again so the reverse reaction could proceed. The LTJ is designed with a relatively large expansion volume so the reaction occurs near isothermally while the pressure steadily rises by a fraction of a bar. The nature of an LTJ experiment mimics the reaction behaviour in a resorption machine. A complete cycle can be seen in Fig. 9. The temperatures and pressure are plotted against time, with the pressure scale on the right-hand y axis. The temperature jump effect is observed at around five seconds (to initiate desorption) can be seen as the 'LTJ Wall' temperature rising sharply as the baths are switched, then the adsorption cycle begins at two hundred and fifty seconds with a jump in the reverse direction.

3.1.1. Superheated Metastate

During the cycle, the temperature reading of the sample tracks the reactor wall temperature until the phase change conditions are met. Rather than the process temperature reaching a stationary value at onset of reaction, a metastable superheated state occurs. The temperature briefly exceeds the equilibrium conditions, before returning when the reaction initiates. This is similar to behaviour observed in phase change materials and the authors hypothesise a similar effect, where initiation requires more energy to cause the crystalline lattice structure to reform, but once overcome the phase change proceeds as expected. The superheat behaviour can be observed in the cycle plot in Fig. 9. The metastable state is visible on the red plot (ENG) as the local maximum at around 20 seconds for the desorption reaction and similarly can be seen as a local minimum at around 260 seconds for the adsorption reaction.

3.1.2. Heat Transfer Limited Rate of Reaction

In Fig. 9, the desorption temperature jump can be seen to occur at 5

Table 1
Salt preparation data, a,b,c tube side and d,e,f are shell side tests (test f used water as the heat transfer fluid).

Test configuration	Tube			Shell		Shell Water test
Salt	$MnCl_2$	$BaCl_2$	$BaCl_2$	$MnCl_2$	$BaCl_2$	$BaCl_2$
(Prepared with)	$MnCl_2$●$4H_2O$	$BaCl_2$●$2H_2O$	$BaCl_2$●$2H_2O$	$MnCl_2$●$4H_2O$	$BaCl_2$●$2H_2O$	$BaCl_2$●$2H_2O$
Weight Dry Salt (g)	0.791	0.586	0.655	4.038	2.936	3.095
Weight ENG (g)	0.651	0.639	0.649	2.594	2.556	2.008
Solution (g/100 ml)	150	43	36	150	43	44.3
Diameter (mm)	10.88	10.88	10.88	34.5	34.5	31.5
Inner Diameter (mm)	1	1	1	12.7	12.7	12.7
Length (mm)	9.5	9.5	9.5	9.5	9.5	9.5
Number of discs	5	5	5	2	2	2
Test	a	b	c	d	e	f

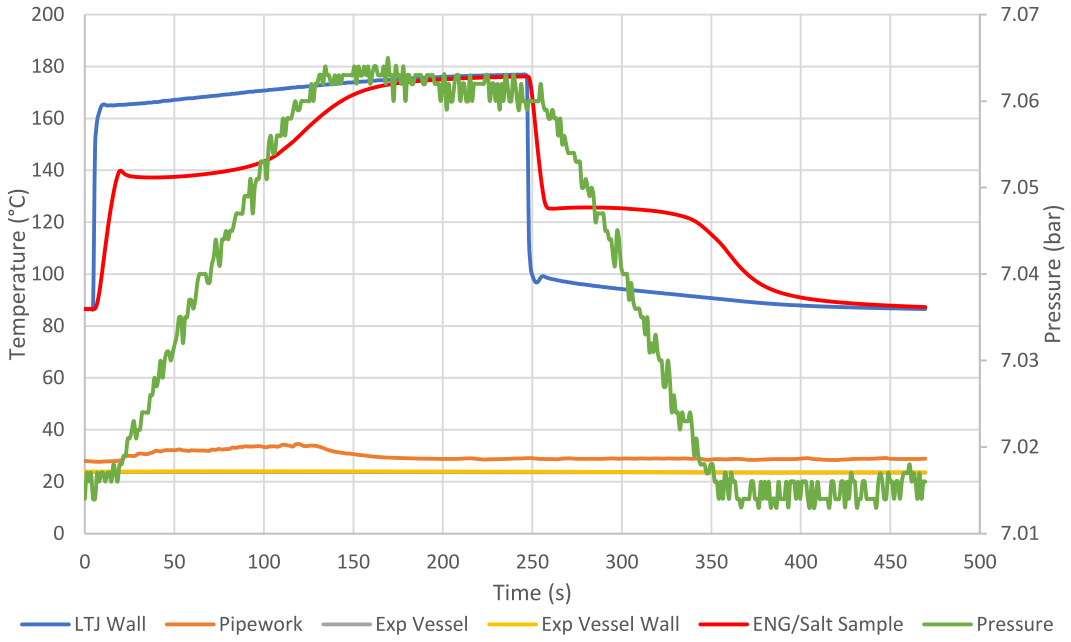

Fig. 9. LTJ tube-side cycle of manganese chloride (test a), desorption followed by adsorption. Pressure on the right-hand scale. The legend values are as follows: LTJ wall is TIT L1; Pipework is TIT PW1; Exp Vessel is Expansion volume TIT E2; Expansion Vessel wall is the expansion vessel wall reading TIT E1; ENG is the temperature of the centre of the sample or surface TIT L2 (and in the shell, also TIT L3).

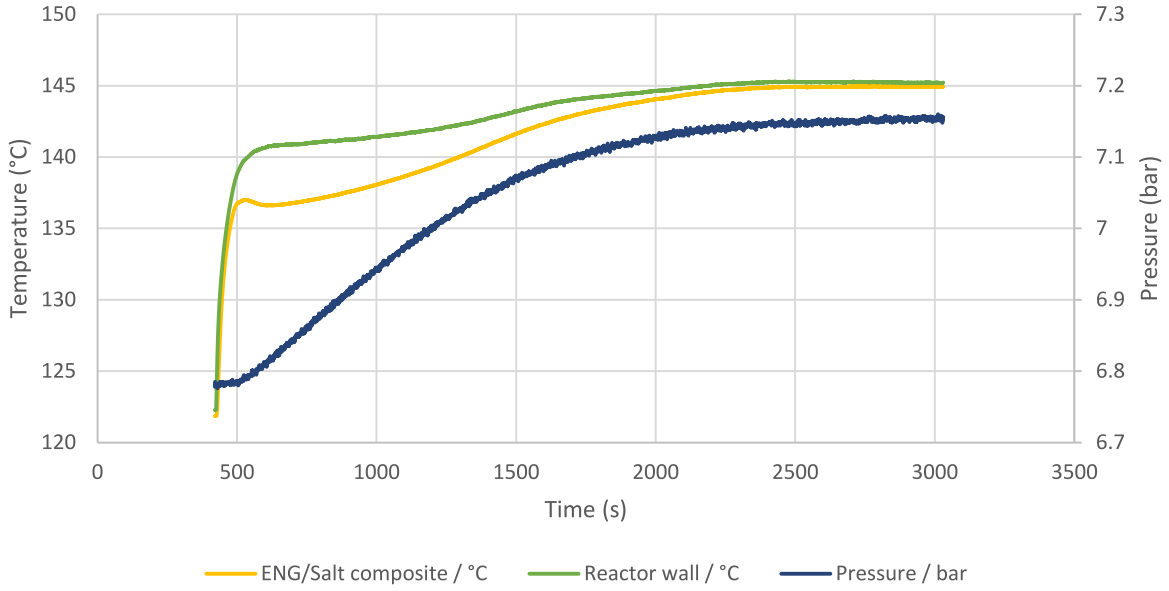

Fig. 10. Shell-Side test for manganese chloride. Temperature of the ENG composite is an average of the two thermocouples TIT L1&L2 (test d).

seconds. The material temperature (ENG/Salt Sample) follows the wall temperature quickly as expected. Once the change in equilibrium conditions occurs (after the peak), the pressure rise is observed as the reaction begins. The pressure rise is at a constant rate between the onset and completion for both adsorption and desorption, this shows the reaction is limited by the rate of heat transfer. If mass transfer or the chemical reaction were limiting the rate, the reaction profile would not appear linear between a maximum (pressure) or minimum (pressure), in both adsorption and desorption. Additionally, the later successful validation of the model which neglects mass transfer supports this conclusion.

The reaction for all intents and purposes is defined by the linear changes between the two constant pressures as described, but a full stoichiometric change in the pressure is not achieved. The reaction continues (particularly adsorption, if the process is left overnight) but is at a negligible rate. It is assumed that there is an active fraction of salt/ammoniate that is '*available*' to react; i.e., the crystal grains are well distributed and small enough due to the matrix, that there is a fixed grain surface area where the reaction readily happens. The remainder is not readily available for reaction, perhaps being trapped in inaccessible pores. The active fraction values found are consistent between tube and shell side tests and do not appear to deteriorate over the number of cycles performed.

3.1.3. *Shell Side tests*

Fig. 10 and Fig. 11 show two different shell side tests. Some of the characteristics described within the tube side LTJ can still be seen such as the superheating effect. In Fig. 10 there is some pressure rise due to

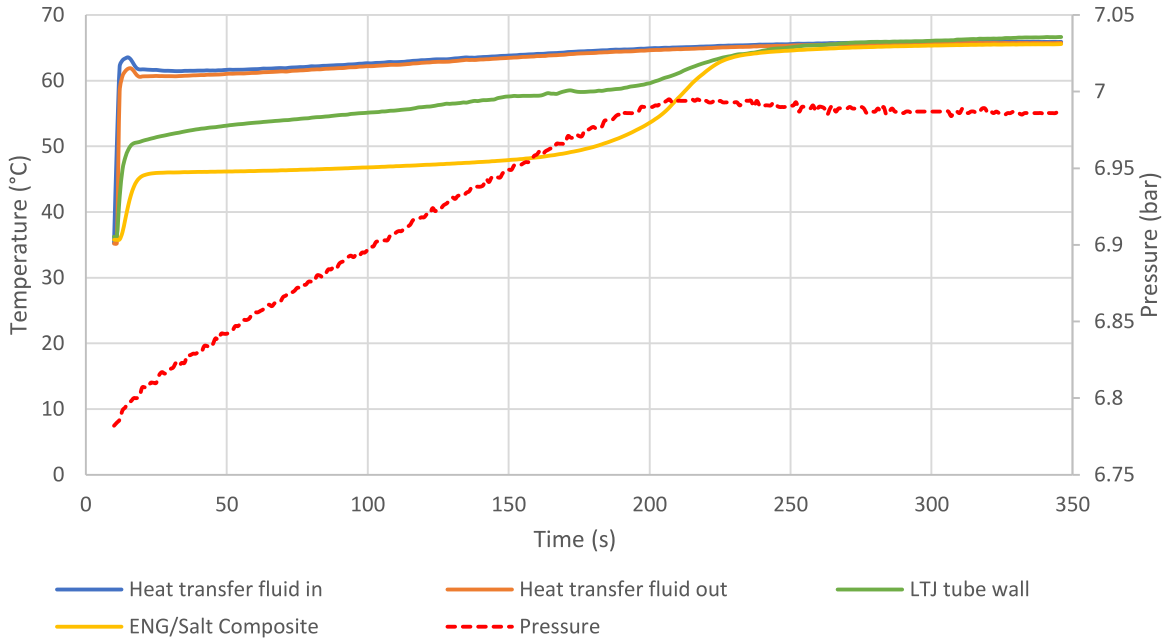

Fig. 11. Shell side test for barium chloride (test f). This time the LTJ was heated with water and had improved heat transfer, also the sample had a smaller central hole. This was a test with improved heat transfer, leading to a large reduction in heating time. The simulation of these results can be seen in Appendix D, Fig. D2.

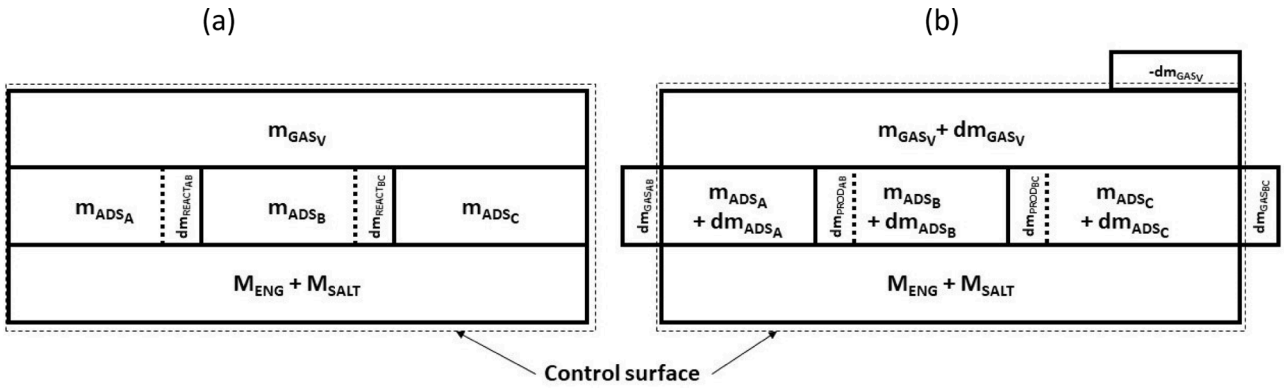

Fig. 12. Unit cell masses at time t (a) and time t + dt (b)

heating observed between 2000 and 3000 seconds. This is because the reaction has occurred over a much longer time period and the substantial thermal mass of the reactor becoming hot and heating the gas in the system. This is avoided in the test shown in Fig. 11.

To improve the heat transfer to the sorbent and to improve the reaction rate (as relating to the point in section 3.1.2), some discs were cut with a custom hole saw to have a smaller central hole in order to achieve a tighter fit and therefore reduced heat transfer resistance between the sample and the tube wall. In Fig. 11 the result can be seen; a much faster rate of reaction, a more constant temperature reading on the composite during the cycle, and a very clear constant pressure rise. This further highlights the heat transfer limitation of the reaction rate.

The cycle in Fig. 11 *test f*, shows discs of a size in the range that might be used in a real device, and this time water was used as the heat transfer fluid. The reaction time is much faster than results observed elsewhere in literature which is promising for a real machine. Thermocouples have been added to measure the fluid inlet and outlet temperatures to the reactor. The temperature difference between fluid and the central tube wall is similar to the difference between the wall and the outside radius of the ENG implying significant fluid-side heat transfer resistance. The heat transfer fluid was silicone oil in Fig. 9, Fig. 10, and water in Fig. 11. In the silicone oil tests there was laminar flow and poorer heat transfer. However, in none of the tests is the fluid temperature or fluid heat transfer of great importance to the analysis; since the model only encompasses the heat flow from the wall at known temperature (a boundary condition) to the furthest radius of ENG.

3.2. Simulation Methodology

In order to characterise the salt-ENG reaction behaviour, a finite difference model has been developed. To match the geometry in the tube and shell side reactor, the model is based on a cylindrical structure in which the composite ENG with its impregnated salt is either externally heated or cooled within a tube (tube-side), or internally heated from a central tube (shell-side). Any number of radial nodes can be used but only one axial node. Conduction heat transfer is assumed between elements, and the heat transfer between the tube wall and the adjoining node is simulated by the resistance of a static ‘gap’ layer of gaseous ammonia between the two. For each time step the heat fluxes into and out of each element are calculated; this is ultimately what drives the adsorption or desorption. An estimated pressure rise is assumed for the time step which must be iterated to arrive at the final value. Chemical reaction rate equations are used to determine the masses of ammoniated complexes changing from one state to another using the assumed

(a)

m_{ADS_A}	m_{ADS_B}	m_{ADS_C}
m_{SALT_A}	m_{SALT_B}	m_{SALT_C}

(b)

$m_{ADS_A} + dm_{ADS_A}$	$m_{ADS_B} + dm_{ADS_B}$	$m_{ADS_C} + dm_{ADS_C}$
$m_{SALT_A} + dm_{SALT_A}$	$m_{SALT_B} + dm_{SALT_B}$	$m_{SALT_C} + dm_{SALT_C}$

Fig. 13. Unit cell salt and adsorbate masses at time t (a) and time t + dt (b)

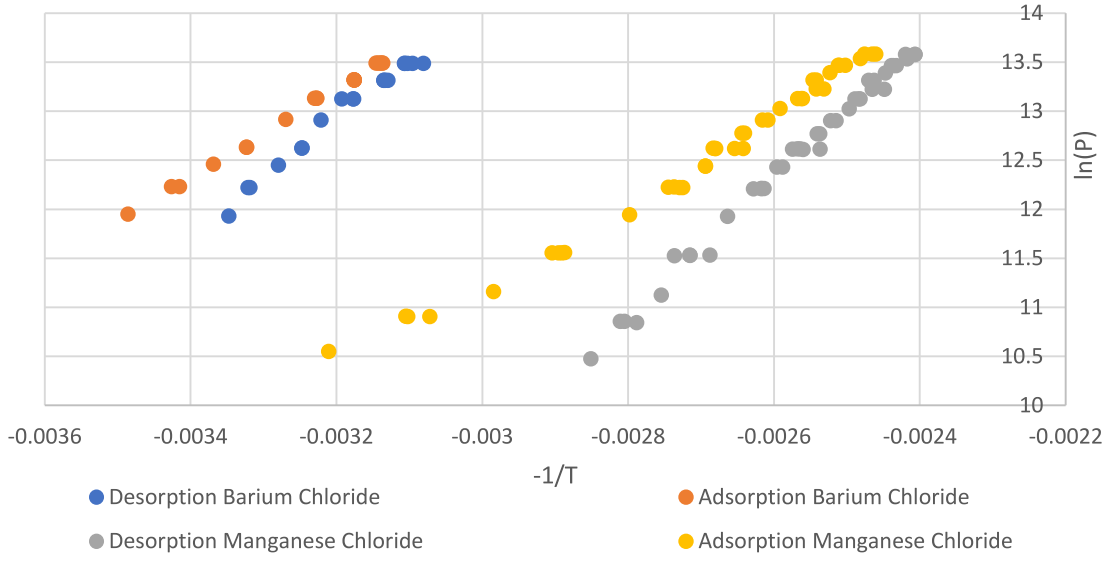

Fig. 14. Data points for salt reaction isosteres

Table 2
Enthalpy and entropy values for non-equilibrium (hysteresis) lines and heat of reaction from equilibrium line.

Salt	$MnCl_2$	$BaCl_2$
NH_3 mole change	6-2	8-0
Δ*h* adsorption (kJ/kmol)	36611.107	37360.200
Δ*s*adsorption (kJ/kmol K)	202.865	229.454
Δ*h* desorption (kJ/kmol)	58196.253	48924.790
Δ*s* desorption (kJ/kmol K)	253.641	263.993
Measured Δ*h* heat of reaction (kJ/kmol)	42523.900	40745.437

pressure rise and current progression of the reactions taking place. This enables the temperature changes in the nodes to be calculated using an energy balance. It is then possible to calculate the total mass of ammonia (gaseous or adsorbed) in the system. This must of course be constant, and the estimated pressure rise is varied (using the MATLAB® fzero function) until this is between prescribed limits.

3.2.1. Energy balance of a unit cell

Fig. 12 shows a discretised unit cell of ENG impregnated with salt and possibly also containing solid adsorbate. The diagram illustrates how the model conceptualises the changes during sorption in a lumped parameter model, illustrating the change in a single unit cell or element. Between times *t* and *t*+*dt*, a mass of adsorbate $dm_{REACT_{AB}}$ in the form of A (indicated by the left-hand dotted line in a) has reacted to form adsorbate in the form B. Simultaneously, a mass of adsorbate $dm_{REACT_{BC}}$ in the form of B (indicated by the right-hand dotted line in a) has reacted to form adsorbate in the form C. These might be, for example, $CaCl_2$•$8NH_3$, $CaCl_2$•$4NH_3$ and $CaCl_2$•$2NH_3$. The model accounts for gas flow to or from the control volume and the resultant change in pressure. The model copes with either all the adsorbate reacting from form A to B before B to C or the situation when both transitions occur simultaneously, as seen in salts like $CaCl_2$, as observed by van der Pal (van der Pal and Critoph, 2017). The approach here applies the same reaction equation for both phase changes and therefore differs to the work by Mazet, et al. (Mazet et al., 1991).

The unit cell is small enough to be used in a finite difference program that assumes it is all at the same temperature and pressure. The unit cell volume is fixed but can be any geometry: cylindrical, rectangular, etc. The ENG and the un-ammoniated salt are characterised by their mass, density and specific heat and the whole volume has a fixed conductivity, nominally that of the ENG matrix. There are also masses of adsorbate types A, B, C (e.g. .$8NH_3$, .$4NH_3$ and .$2NH_3$) which have their own densities and specific heats, assumed at the moment to be those of solid ammonia as observed by Hirata and Fujioka, and Fujioka et al. (Fujioka et al., 1996; Hirata and Fujioka, 2003). Considering desorption between time *t* and *t* + *dt*, a small mass of type A, $m_{REACT_{AB}}$ reacts, some being converted to $m_{PROD_{AB}}$ and the remainder becoming gas $dm_{GAS_{AB}}$, which leaves the control volume. Some of type B reacts to form type C plus some expelled gas in similar fashion. There is also a gas void volume within the control volume, being the ENG pore volume not occupied by salt (fixed), or adsorbate (variable). Changes in pressure and temperature will affect m_{GAS_V}, the mass of gas in the void volume, as well as any portion of it leaving the volume, - dm_{GAS_V}.

The first law for the unsteady control volume in desorption is

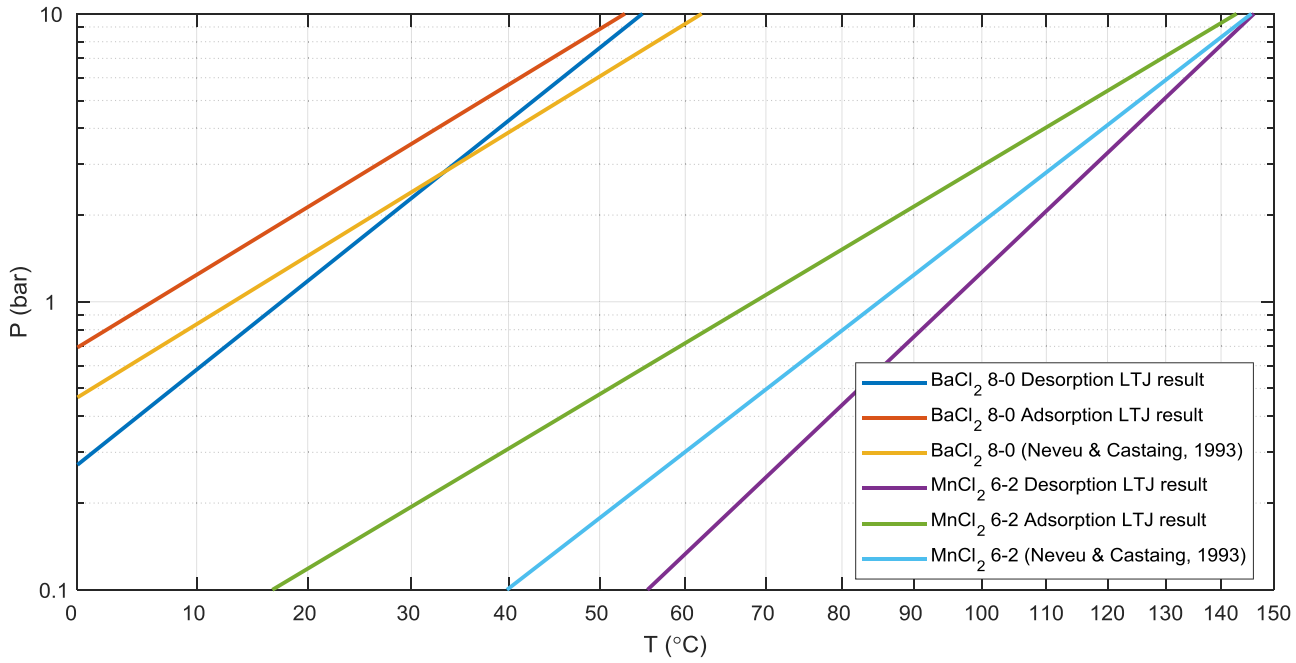

Fig. 15. Clapeyron plots of experimental results versus results from literature (Neveu and Castaing, 1993)

$$\begin{aligned}\Delta Q &= \Delta U_{ENG} + \Delta U_{SALT} + \Delta U_{ADS} + \Delta U_{GAS_V} + dm_{GAS_{AB}} h_{out} + dm_{GAS_{BC}} h_{out} - dm_{GAS_V} h_{out} \\ &= MC_p dT + \Delta U_{ADS_A} + \Delta U_{ADS_B} + \Delta U_{ADS_C} + \Delta U_{GAS_V} + dm_{GAS_{AB}} h_{out} + dm_{GAS_{BC}} h_{out} - dm_{GAS_V} h_{out}\end{aligned} \tag{1}$$

where ΔQ is the total heat entering the control volume in time dt.

The terms are either changes in internal energy U of the different masses of ENG, salt, adsorbate and gas within the control volume, or the enthalpy of the masses of gas entering or leaving the control volume. The MC_p term is the thermal mass (J/K) of the ENG plus the salt, whether accessible to the reaction or not. In desorption, ΔQ is positive and the enthalpy of the outlet streams h_{out} is that for the control volume temperature. In adsorption, ΔQ is negative and h_{out} is for the temperature of the incoming gas, which in an LTJ experiment is the expansion vessel temperature T_E.

The terms can be considered separately: that associated with type A and conversion to/from B and the gas entering or leaving, that associated with type B and conversion to/from C and the gas entering or leaving, the sensible heating of C, and the sensible heating of the salt and ENG.

First considering type A:

$$\begin{aligned}&(\Delta U_{ADS_A} + dm_{GAS_{AB}} h_{out}) \\ &= \Delta U_{NR-ADS_A} + \Delta U_{R-ADS_A} + dm_{GAS_{AB}} h_{out} \\ &= \Delta(mu)_{NR-ADS_A} + \Delta(mu)_{R-ADS_A} + dm_{GAS_{AB}} h_{out} \\ &= m_{NR-ADS_A} du_{NR-ADS_A} + dm_{PROD_{AB}} u_B - dm_{REACT_{AB}} u_A + dm_{GAS_{AB}} h_{out} \\ &= (m_{ADS_A} - dm_{REACT_{AB}}) c_{V_{ADS}} dT + dm_{PROD_{AB}} (h_B - pv_{ADS_B}) \\ &\quad - dm_{REACT_{AB}} (h_A - pv_{ADS_A}) + dm_{GAS_{AB}} h_{out} \\ &= m_{ADS_A} c_{V_{ADS}} dT + dm_{GAS_{AB}} \Delta h_{AB} - dm_{PROD_{AB}} pv_{ADS_B} + dm_{REACT_{AB}} pv_{ADS_A}\end{aligned} \tag{2}$$

where subscripts NR and R indicates non-reacting and reacting; and subscripts $PROD$ and $REACT$ indicate product (time t+dt) and reactant (time t). Δh_{AB} is the enthalpy of reaction per unit mass.

Given that:

$dm_{REACT_{AB}} = dm_{ADS_A}$ The only change in dm_{ADS_A} is due to the AB reaction.

$dm_{PROD_{AB}} = dm_{ADS_A} \times \frac{B}{A}$ Change from .A mols to .B mols

$pv_{ADS_A} = pv_{ADS_B} = pv_{ADS}$ Specific volume of all ammoniate assumed equal to that of solid NH_3.

Then:

$$\begin{aligned}\Delta U_{ADS_A} + dm_{GAS_{AB}} h_{out} &= m_{ADS_A} c_{V_{ADS}} dT + dm_{GAS_{AB}} \Delta h_{AB} \\ &\quad + dm_{ADS_{AB}} pv_{ADS} \left(1 - \frac{B}{A}\right)\end{aligned} \tag{3}$$

The first term on the right-hand side of the equation is sensible heating of adsorbate A, the second is the reaction enthalpy term. The third term is the work associated with shrinkage or expansion; the term is quite small although the expansion of adsorbate can be considerable. Keeping account of the changing volume of solid within the control volume is important since expansion of the solid reduces the gas space available and expels gas from the control volume. The flow work done by gas expelled from the control volume is accounted for by h_{out}. It is preferred to keep small terms for completeness since they do not slow the numerical solution significantly.

A similar argument applies to the terms in Eq. (1) relating to conversion between forms B and C:

$$\begin{aligned}\Delta U_{ADS_B} + dm_{GAS_{BC}} h_{out} &= m_{ADS_B} c_{V_{ADS}} dT + dm_{GAS_{BC}} \Delta h_{BC} \\ &\quad + dm_{ADS_{BC}} pv_{ADS} \left(1 - \frac{C}{B}\right)\end{aligned} \tag{4}$$

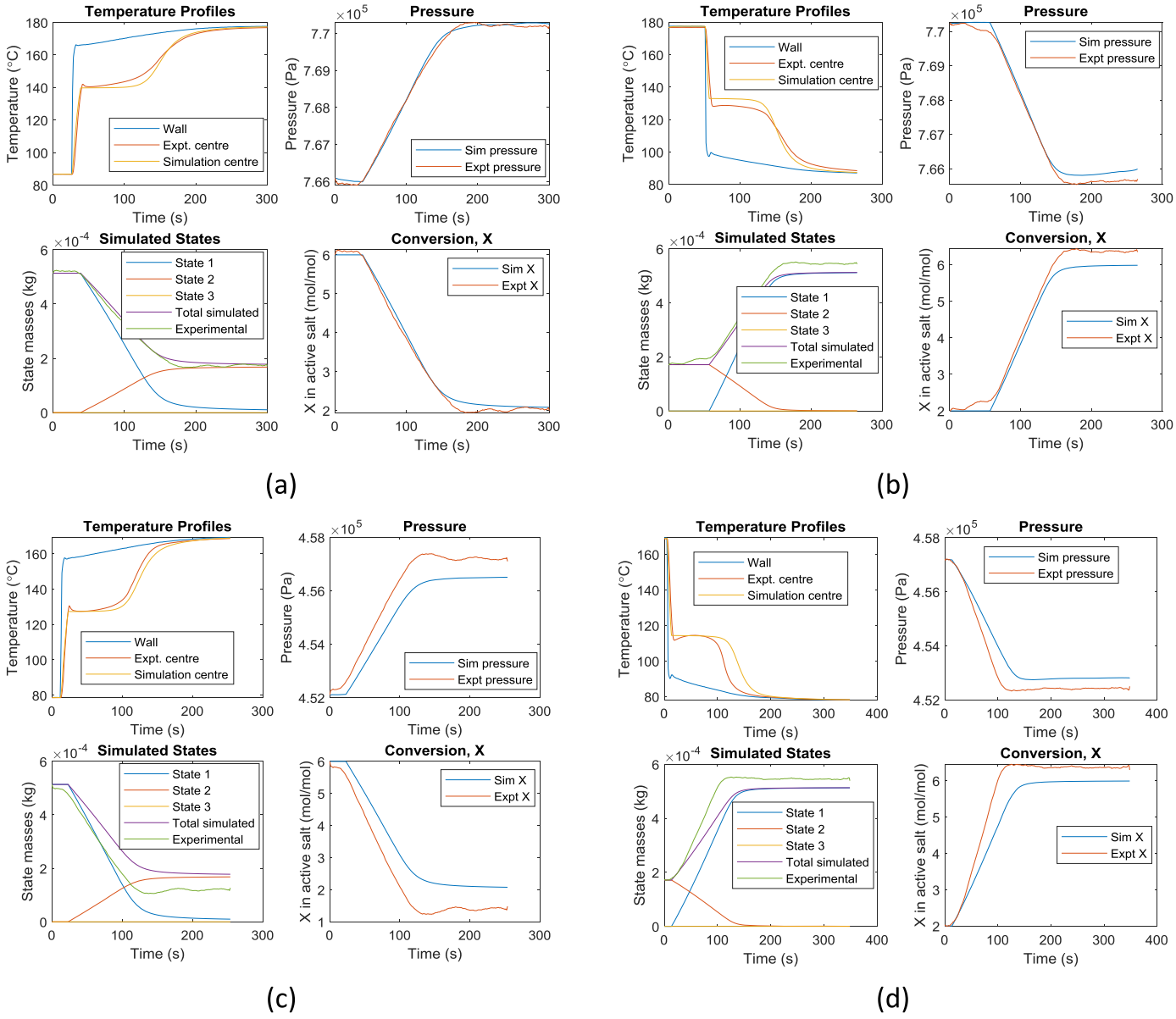

Fig. 16. Simulation results plotted against experimental results from the tube-side LTJ testing manganese chloride (test a): (a) Desorption at 7.6 bar; (b) adsorption at 7.6 bar; (c) desorption at 4.5 bar; and (d) adsorption at 4.5 bar. The plots comprise of 4 graphs, the temperatures, system pressure, the masses in each state and the conversion of the material.

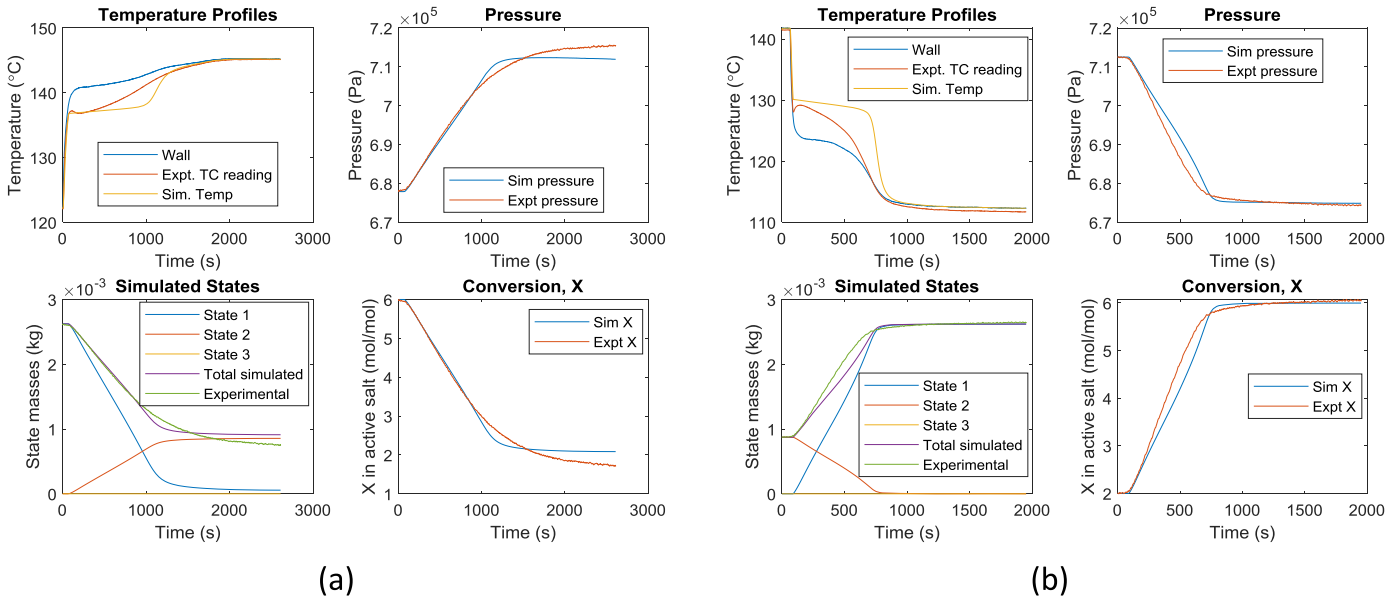

Fig. 17. Simulations of the shell-side reactor plotted against the experimental results for manganese chloride (test d): (a) desorption; (b) adsorption. The temperature reading is less accurate, perhaps due to the sampling on the material surface, but the rate of reaction is very accurate.

The remaining terms in Eq. (1) are:

$$\Delta U_{ADS_C} = m_{ADS_C} c_{V_{ADS}} dT \tag{5}$$

Sensible heat only; there is no C to D reaction considered.

And for the gas void volume:

$$\begin{aligned}\Delta U_{GAS_V} - dm_{GAS_V} h_{out} &= \Delta(mu)_{GAS_V} - dm_{GAS_V} h_{out} \\ &= m_{GAS_V} du_{GAS_V} + u_{GAS_V} dm_{GAS_V} - dm_{GAS_V} h_{out} \\ &= m_{GAS_V} c_{V_{GAS}} dT + dm_{GAS_V}(u_{GAS_V} - h_{out}) \\ &= m_{GAS_V} c_{V_{GAS}} dT - pv_{GAS_V} dm_{GAS_V}\end{aligned} \tag{6}$$

The first term is the change in internal energy and the second is the positive work done in expansion.

Now if all the separate terms are substituted into Eq. (1) we obtain:

$$\begin{aligned}dQ = {} & MC_p dT + (m_{ADS_A} + m_{ADS_B} + m_{ADS_C}) c_{V_{ADS}} dT + dm_{GAS_{AB}} \Delta h_{AB} \\ & + dm_{ADS_{AB}} pv_{ADS}\left(1 - \frac{B}{A}\right) + dm_{GAS_{BC}} \Delta h_{BC} + dm_{ADS_{BC}} pv_{ADS}\left(1 - \frac{C}{B}\right) \\ & + m_{GAS_V} c_{V_{GAS}} dT - dm_{GAS_V} pv_{GAS_V}\end{aligned} \tag{7}$$

The first line is sensible heating/cooling of ENG, salt and adsorbate, the second is reaction and expansion work in AB, the third is reaction and expansion work in BC, and the fourth is sensible heating and expansion of the gas.

dm_{GAS_V} may be calculated from perfect gas law assumptions and the pressure and temperature changes. If the expelled volume due to gas void temperature change dT and pressure change dp is dV:

$$dV_{GAS_V} = V_{GAS_V}\left(\frac{\frac{dT}{T} - \frac{dp}{p}}{1 + \frac{dp}{p}}\right) = dm_{GAS_V} v_{GAS_V} \tag{8}$$

which is substituted into Eq. (7) to give:

$$\begin{aligned}dQ = dT & \left(MC_p + \sum_A^C m_{ADS} c_{V_{ADS}} + m_{GAS_V} c_{V_{GAS}} - \frac{\frac{pV_{GAS_V}}{T}}{1 + \frac{dp}{p}}\right) + dm_{GAS_{AB}} \Delta h_{AB} \\ & + dm_{ADS_{AB}} pv_{ADS}\left(1 - \frac{B}{A}\right) + dm_{GAS_{BC}} \Delta h_{BC} + dm_{ADS_{BC}} pv_{ADS}\left(1 - \frac{C}{B}\right) \\ & + \frac{dpV_{GAS_V}}{1 + \frac{dp}{p}}\end{aligned} \tag{9}$$

Eq. (9) is dominated by the heat of reaction term, for this reason, constant (mean) values of specific heat were taken since any error would be negligible. Future modelling at scale with larger temperature swings should consider incorporating variations of specific heat with temperature.

For the purposes of simulating the process in a program, this is rearranged to solve for dT:

$$dT_{des} = \frac{\begin{pmatrix} dQ - dm_{GAS_{AB}} \Delta h_{AB} - dm_{ADS_{AB}} pv_{ADS}\left(1 - \frac{B}{A}\right) - dm_{GAS_{BC}} \Delta h_{BC} \\ - dm_{ADS_{BC}} pv_{ADS}\left(1 - \frac{C}{B}\right) - \frac{dpV_{GAS_V}}{1 + dp/p} \end{pmatrix}}{\left(MC_p + \sum_A^C m_{ADS} c_{V_{ADS}} + m_{GAS_V} c_{V_{GAS}} - \frac{\frac{pV_{GAS_V}}{T}}{1 + dp/p}\right)} \tag{10}$$

The analysis is slightly different in adsorption when gas entering the control volume (generally in an LTJ test) can cool it.

The equation for dT becomes:

$$dT_{ads} = \frac{\begin{pmatrix} dQ - dm_{GAS_{AB}} \Delta h_{AB} - dm_{ADS_{AB}} pv_{ADS}\left(1 - \frac{B}{A}\right) - dm_{GAS_{BC}} \Delta h_{BC} \\ - dm_{ADS_{BC}} pv_{ADS}\left(1 - \frac{C}{B}\right) - \frac{dpV_{GAS_V}}{1 + \frac{dp}{p}} + \\ m_{GAS_V} \frac{\frac{dp}{p}}{1 + \frac{dp}{p}} c_p (T - T_E) \end{pmatrix}}{\left(MC_p + \sum_A^C m_{ADS} c_{V_{ADS}} + m_{GAS_V} c_{V_{GAS}} - \frac{\frac{pV_{GAS_V}}{T}}{1 + \frac{dp}{p}} + m_{GAS_V} \frac{\frac{1}{T}}{1 + \frac{dp}{p}} c_p (T - T_E)\right)} \tag{11}$$

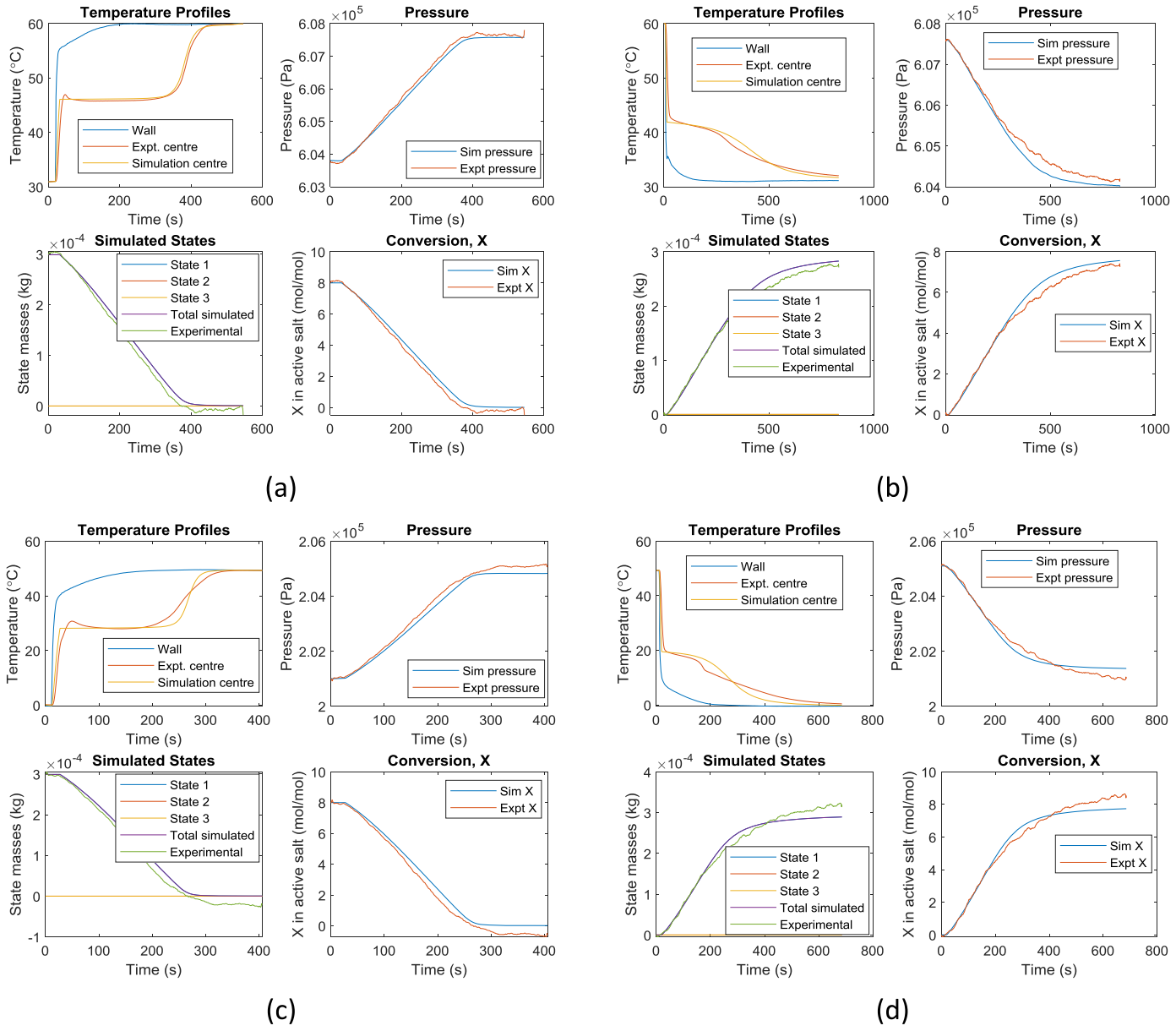

Fig. 18. Simulation results plotted against experimental results from the tube side LTJ testing barium chloride (test b): (a) Desorption at 6 bar; (b) adsorption at 6 bar; (c) desorption at 2 bar; and (d) adsorption at 2 bar. The plots comprise of 4 graphs, the temperatures, system pressure, the masses in each state and the conversion of the material.

The final terms in both numerator and denominator account for the sensible heating or cooling of gas entering the control volume at temperature T_E.

Whilst complicated, given an assumed pressure rise the change in temperature and then the mass of ammonia in gaseous or adsorbed states A, B, and C can be calculated.

3.2.2. Reaction rate equations

In Fig. 13 the m_{ADS} terms are the masses of adsorbate of types .A mols, .B mols and .C mols of adsorbed ammonia and the m_{salt} terms are the masses of salt associated with the A B and C forms.

The reaction rate equations used are based on those of Mazet et al. (Mazet and Amouroux, 1991; Mazet et al., 1991):

$$\frac{dX}{dt} = (1-X)^n A_r \frac{p_{eq} - p}{p} \tag{12}$$

where:

X is the advancement of the reaction (from zero to unity)
p is the pressure
p_{eq} is the equilibrium pressure
A_r and n are constants. $A_r$is an Arrhenius term that is actually a function of temperature but may be successfully assumed constant over the ranges used in this work.

Whilst generally used in molar form the same numerical values of A_r and n apply when using mass formulation. Thus, when expressing reaction AB in differential form:

From .A to .B (desorbing)

$$\frac{dm_{SALT\ A\ to\ B}}{dt} = (m_{SALT\ A} + m_{SALT\ B})\left(\frac{m_{SALT\ A}}{m_{SALT\ A} + m_{SALT\ B}}\right)^{n_{AB}} A_{rAB} \frac{p_{eq\ AB} - p}{p} \tag{13}$$

From .B to .A (adsorbing)

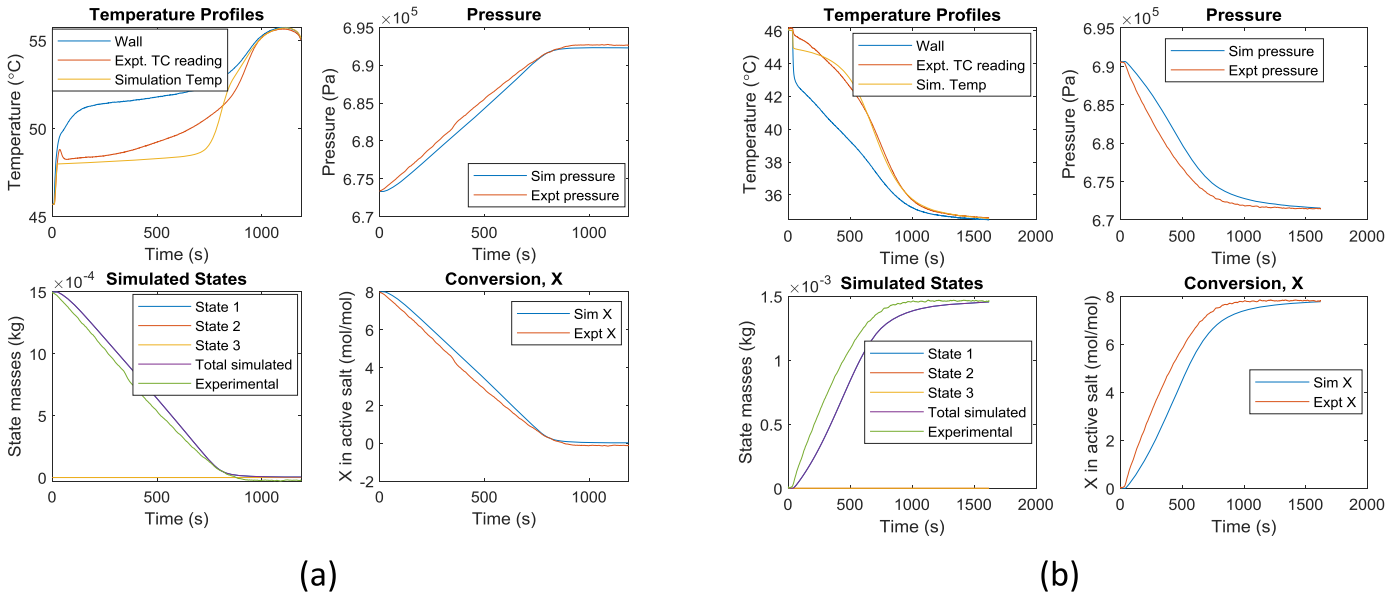

Fig. 19. Simulation of shell side barium chloride results: (a) desorption; (b) adsorption. The wall temperature is held by the phase change temperature (test e). A nominal gap of 0.035 mm was observed in the simulation.

Table 3
Constants in the model – Eqs. (13 & 14)

Salt	$MnCl_2$	$BaCl_2$
NH_3 mole change	6-2	8-0
A_r adsorption	2	2
n adsorption	3	0.1
n desorption	3	2
A_r desorption	3	3
Active Fraction	0.8	0.78

$$\frac{dm_{SALT\ B\ to\ A}}{dt} = (m_{SALT\ A} + m_{SALT\ B})\left(\frac{m_{SALT\ B}}{m_{SALT\ A} + m_{SALT\ B}}\right)^{n_{BA}} A_{rBA}\frac{p_{eq\ BA} - p}{p} \tag{14}$$

Similarly, for the BC reaction:
From .B to .C (desorbing)

$$\frac{dm_{SALT\ B\ to\ C}}{dt} = (m_{SALT\ B} + m_{SALT\ C})\left(\frac{m_{SALT\ B}}{m_{SALT\ B} + m_{SALT\ C}}\right)^{n_{BC}} A_{rBC}\frac{p_{eq\ BC} - p}{p} \tag{15}$$

From .C to .B (adsorbing)

$$\frac{dm_{SALT\ C\ to\ B}}{dt} = (m_{SALT\ B} + m_{SALT\ C})\left(\frac{m_{SALT\ C}}{m_{SALT\ B} + m_{SALT\ C}}\right)^{n_{CB}} A_{rCB}\frac{p_{eq\ CB} - p}{p} \tag{16}$$

The change in the salt mass is readily used to calculate the new values of all the masses of salt and adsorbate plus the masses of gas adsorbed or desorbed at the next time step, taking account of conditions under which the masses of .B may be the result of simultaneous A to B and B to C reactions.

The derivation of this model goes back to fundamentals when looking at simultaneous reactions, and enables the model to replicate reaction behaviour over a number of conditions accounting for different phase changes. Mazet et al. presented Eq. 12 and for subsequent reactions presented this kinetic equation Eq. 17 with Y describing the extent of the second reaction:

$$\frac{dY}{dt} = ([1 - Y]X)^n \cdot A_r \cdot \frac{p - p_{eq}}{p} \tag{17}$$

The results presented by Mazet et al., (Mazet et al., 1991) report that the constants ($A_r$and n) vary depending on conditions. They quote: 'These remarks do not therefore allow us to obtain coefficients which are valid over the whole range of experimental constraint temperatures at a given pressure p. It would therefore seem that a phenomenon influencing the rate of reaction has not been taken into account in the model.' In this study, the composite material and the detailed approach in modelling with attention to the heat transfer shows that the rate of heat transfer is the limiting factor and single values of A_r and n are identified. This contradicts the work by Mazet et al., and by identifying single parameters differs from other literature (Jegede, 2017; Wu et al., 2019; Yuan et al., 2019). This approach has also been tested in adsorption, and a similar single value for each constant has been identified, but the values differ between adsorption and desorption.

3.3. Hysteresis and heats of reaction

Ideally there is a single equilibrium line that relates the pressure and temperature of the reaction, whether adsorption or desorption. The well-known relationship is given by:

$$ln(p) = \frac{\Delta s}{R} - \frac{\Delta h}{RT} \tag{18}$$

Where Δs is the change in entropy J/kg K, Δh is the enthalpy of reaction in J/kg, T is temperature in Kelvin and $R$is the gas constant in J/kg K. Measurement of the line experimentally is normally used to determine the heat of reaction via the slope. However, salt-ammonia reactions in real applications and with realistic reaction speeds exhibit hysteresis with adsorption and desorption at the same pressure occurring at up to 10 degrees or more apart. The position of the separate adsorption and desorption lines can be measured experimentally in LTJ tests, as described in the following section of this paper. A complication is that in general the two lines do not have the same slope. In this case the slope cannot in any case be used to calculate reaction heats since equation 18 assumes the process to be reversible and hysteresis is of course irreversible.

If a cycle of a) isobaric heating from the adsorption line (fully adsorbed) to the desorption line (fully desorbed), then b) isobaric cooling back to the original state is considered, it can be shown that:

$$\Delta h_{ads} - \Delta h_{des} = \Delta T_{HYS}(c_{v\ ADS} - c_{v\ GAS}) \tag{19}$$

where the term on the left is the difference between the adsorption and desorption enthalpy changes and the term on the right is the difference in the sensible heat of the gaseous and adsorbed ammonia phases when changing in temperature by ΔT_{HYS}, the temperature difference between the desorption and adsorption lines at that pressure. If typical values for the salts under consideration are inserted Δh_{ads} and Δh_{des} differ by only as much as one part in a thousand and so for practical purposes the model considers them equal.

Finding a unified value for Δh was done by employing very slow heating rates and minimal expansion gas volume in as close to an isosteric process as possible, ensuring a large pressure and temperature swing up and down the isostere without completing the reaction, ideally (in the case of zero gas volume) no actual adsorption or desorption occurring. The results are described in section 3.4.1, and a value can be seen between the Δh_{ads} and Δh_{des} observed for the onset of reaction.

3.4. Analytical results

3.4.1. Equilibrium data

Data points were collected after the metastate (discussed in section 3.1.1.) across tests in the tube side reactor to plot the Clapeyron functions for the change in equilibrium. These are plotted in Fig. 14.

Because the change in equilibrium conditions occurs after the metastate at a different temperature, traditional gravimetric methods miss the actual phase change conditions. They do not measure the material temperature, rather the heating temperature provided to the material, therefore the mass change will be observed at the metastate beyond the equilibrium conditions and will not reflect the reaction temperatures that will be observed in large scale machines. Reduced hysteresis was observed by van der Pal and Critoph when cycling a single large scale reactor; the salt could be seen to reach equilibrium at a position along the isostere after heating or cooling steps (van der Pal and Critoph, 2017), highlighting the need for care when dealing with these phenomena in the dynamics.

A best fit was taken from the data points to present a best approximation for the onset of the reaction, providing a basis for modelling the behaviour. From this Δh and Δs values were derived as shown in Table 2 and the isosteres have been plotted in Fig. 15 against the data from Neveu and Castaing. These lines can be used to accurately predict the onset of reaction, but at higher pressures the lines appear to cross; this is an impossibility. Exploration of conditions for onset of reactions would be interesting for adsorption cycles operating at higher working pressures.

The plotted lines illustrate the onset of the reaction but not the enthalpy of reaction, as explained in section 3.3. To investigate the effect of reduced hysteresis and derive the enthalpy of reaction, the LTJ reactor expansion volume was removed and the reactor cycled (heated/cooled) slowly. The effect was to track up and down the equilibrium line. The resulting temperature versus pressure data had reduced hysteresis and the gradients were approximately equal; an average slope of the lines was used to calculate a single value for the heat of reaction. To ensure realistic reaction behaviour when modelling the non-equilibrium data was used to predict the onset of reaction, but the obtained single heat of reaction term used to calculated the heat input and output from the reaction. The single derived enthalpy of reaction can be seen in Table 2. The difference can be observed between those obtained from the Clapeyron relationship at onset of reaction, which highlights the importance of a unified value to abide by the first law of thermodynamics.

3.4.2. Model results

The simulation model discussed in section 4 was computed in MATLAB® in the form of a 1-dimensional finite difference model, discretised in the radial direction; the file is linked in the Research Data section. The model is able to predict the performance of the composite in either tube side configuration such as in Fig. 3, or shell side as in Fig. 7. The MATLAB® program reads the recorded experimental data (wall temperature), and then predicts the rate of reaction, the pressure change and ENG/Salt Sample temperature. The outputs of the simulation were then plotted against the experimental data, as shown in Fig. 16, Fig. 17, Fig. 18 & Fig. 19.

Using the derivations of equation 12 Eqs. 13-(16) in MATLAB®, it was possible to deduce the constants n and A_r, presented in Table 3. This was achieved through trial and error, fitting the simulation result to an experimental result. The simulations were then compared against all experimental test results at different pressures and with differing temperature jumps. The constants identified and used within the model are effective at simulating the kinetics, and particularly effective at predicting the rate of the reaction. Notably, the model holds true in both tube and shell configurations and for different ENG-salt samples.

The first step in fitting the results was done by adjusting an active fraction of the salt so that the pressure rise was equal to a stoichiometric mass of desorbed ammonia. This was calculated from the mass of gas in the expansion volume assuming an ideal gas. Values for active fraction were consistent throughout the results. Further adsorption/desorption may occur but is limited by the rate of diffusion into the crystal or through a product layer. In practice, a starting and finishing point is clearly observed (presenting the mass that is active during the *fast* reactions) and the rate beyond this is very low if not unobservable during the cycles, therefore deemed inactive. In a working machine the ammonia would either stay in the adsorbed state, or not adsorb during a cycle (creating these boundary operating conditions for the active fraction). The consistency in the value between the tests in the tube and the larger shell-side supports this to be true in the ENG-salt composite which largely overcomes mass transfer issues. The second step of fitting was to adjust size of the gap simulating the heat transfer resistance. The gap is adjusted such that the simulated reaction time matches that of the experimental reaction time. Finally, the equation parameters n and A_r are adjusted, with trial and error, to match simulated and experimental data, adjusting the gap if necessary. Once a good fit was obtained, the parameters were tested against the other results and modified if required. The gap was assumed the same for the same sample, but it was assumed that a different gap could occur in different samples particularly when tube and shell are considered. For the model to prove a success, n and A_r would remain constant over all tests of the same salt. The nominal gap sizes found for barium tests for example were 0.15 mm and 0.043 mm for the samples in the tube and the shell respectively. It is worth noting that subsequent tests to improve heat transfer, reduced the nominal gap value to 0.0019 mm; this was done by pushing discs with a smaller central hole onto the tube as in *test f*.

The rate of heat transfer (relative size of the gap) has the greatest effect on the rate of reaction although n and A_r have some effect on the shape. Simulation results from the MATLAB® program can be seen in Fig. 16, Fig. 17, Fig. 18 & Fig. 19. Results from test c, as described in Table 1, can be seen in Appendix C. State 1 equates to state A, state 2, equates to state B and state 3 equates to state C.

When simulating the shell tests, the average of the two outer thermocouples was taken to indicate the ENG/composite temperature within the cylindrical model. The pressure can be seen to continue to rise in Fig. 17 within the shell, which is due to the heating of gases in the void of the reactor. The challenge of the shell side unit cell was to have a reactor design reflective of a heat exchanger, but simple to model. A full-sized machine would have less thermal mass by design as well as being a larger volume filled with as much salt composite as possible, and would likely contain a tube bundle, reducing thermal mass and providing structural stability. The divergence of the temperature reading and simulated temperature in Fig. 12 and Fig. 14 is likely due to the thermocouple being on the outside and in free space against the material as shown in Fig. 7. Thermal resistance between the composite and the thermocouple will also take place. However, the close fit of the pressure curves provides confidence in the results.

To check the validity of the model, a grid independence test for the

number of nodes used in the finite difference model was conducted and can be seen in Appendix A. The simulation results were tested over a range of nodes on both the tube side and larger shell side results. With 2 nodes, the simulation appeared to marginally differ (temperature and pressure profiles), but with more than 2 nodes the results were consistent. The number of nodes within the finite difference model was set to 5. This provided certainty in the accuracy and maintained computational efficiency when considering the time step. The time step needed to be small enough so that the model was stable and was typically between 0.01- 0.005 seconds.

4. Discussion

The active fraction found suggests that around 80% of the salt readily reacts to form an ammoniate during a cycle. The experimental results show the reaction rate is limited by the rate of heat transfer, characterised by a linear pressure change during the adsorption and desorption reactions. It was observed that adjusting the model terms n and A_r have limited effect on reaction rate but influence the shape of the plots, in particular the sigmoidal shape of the temperature curve. The wall heat transfer resistance– modelled by an ammonia gas-filled gap– has the greatest effect on rate, illustrating how it is limited by rate of heat transfer. Mazet and Amouroux suggested the constants n and A_r in their model have no physical meaning and are pseudo in nature (Mazet et al., 1991). They present a range of values for the constants under different conditions, i.e., they are not truly constants. The work in this paper, as well as other work on improved composites such as by (An et al., 2020a) illustrate more accuracy in the prediction of global rates of advancement by similar empirical kinetics functions, with unchanging constants. This is likely a product of better composite materials used, and better experimental instrumentation. The evidence makes further sense when the reaction behaviour is also considered. For example, the ENG matrix ensures a relatively even distribution of grains at a small and constant size while providing void pathway for the gases. When compared with the modelling by Lu et al. which incorporates chemical kinetics, mass transfer into the grain, and heat and mass transfer within the grain; reaction times of hours are observed (Lu et al., 1996). The processes observed testing these salt composites in the LTJ, show short reaction times between 5 and 15 minutes with a linear reaction rate limited by the rate of heat transfer. This empirically shows that the reaction rate (within a somewhat homogenous conductive matrix) is dominated by the deviation from the equilibrium conditions, i.e., the temperature or pressure difference and this is the key component of any kinetic function. This correlates with the limited effect of adjusting n and A_r, only affecting the curvature of temperature and pressure profiles into and out of the constant rate of change.

When the monovariant nature of the reaction is considered, once the equilibrium conditions are overcome, the reaction proceeds in one direction at a constant rate until completion as long as the conditions continue to exceed the equilibrium conditions. Thus the simple advancement model (Eqs. 13-16) predicts reaction kinetics for a resorption machine as the reaction rates are driven by heat transfer or externally imposed changes in pressure. The composite material in this experiment performs well, reducing the rate limiting effects to the thermal resistance between the stainless-steel tube and the composite. The model would appear to predict the reactions for any driving temperature as long as the initial superheating or subcooling effect is overcome so that the reactions initiate. These results suggest, and we conclude, that the rate constants are constants for the application of salt when impregnated in ENG. This provides a good basis for designing a full-size generator since it is now possible to consistently predict the rate of reaction.

Fig. 11 shows the wall temperature at less than 10°C above the reaction temperature of the salt–and the fluid temperature at around 15°C above the reaction temperature–driving the reaction to complete in few minutes, which is promising for reasonable specific power performance. Future work will need to consider the heat transfer from fluid to the tube, ensuring a 10°C driving temperature is possible by reducing resistance between fluid and the tube. This may be possible with enhanced turbulence or increasing tube size to improve heat transfer and will be key to achieving the requirements discussed in section 1.3.

5. Conclusion

LTJ tests have been performed on manganese and barium chloride reacting with ammonia. The salts are embedded in expanded natural graphite and the composite salt performs well with fast cycle times. The results have been modelled using a MATLAB® program that is linked in the research data section.

Key findings are as follows:

- Accurate isosteres are observed and a metastate reported highlighting the importance of LTJ tests over gravimetric methods for ammonia-salt reactions.
- A unified value for the heat of reaction is identified for barium chloride and manganese chloride using a new method.
- A detailed model has been derived going back to the fundamentals of simultaneous reactions and presents a single function for the reaction rate. This has been used to derive the kinetic equation constants A_r and n, and has proven effective for simulating results for wide range of LTJ results between 0.1 and 8 bar.
- The composite presented in this work shows the rate of reaction is limited by the rate of heat transfer; ensuring good heat transfer from fluid to tube, and tube to composite will be key for effective machine performance.
- Cycles of samples sized for practicable machines have been observed to complete in under 10 minutes which shows promise for reasonable power densities.

Test *f* shows improved heat transfer to the samples; however, further research is needed as the heat transfer from the fluid may become a limiting factor, particularly at low driving temperatures. The model successfully predicts the heat transfer and reaction kinetics in both the shell and tube side reactor configurations, highlighting potential for modelling large-scale generators. The next steps in the development of a full-scale machine should consider, the thermal masses, amount of heat transferred and the specific power.

Research Data

The MATLAB® file and an experimental result are deposited in the Warwick Research Archive Portal (WRAP) and are accessible through the following link with a README.TXT file detailing the files. The results from deadweight pressure testing the pressure transducer are also available. Furthermore, thermocouple error testing data can also be seen following the link:http://wrap.warwick.ac.uk/152152/

Declaration of Competing Interest

The authors declare that they have no known competing financial interests or personal relationships that could have appeared to influence the work reported in this paper.

Acknowledgements

This work has been supported by two EPSRC projects: EP/V011316/1, ‘Sorption Heat Pump Systems’ in support of Mission Innovation Challenge 7: Affordable Heating and Cooling, and EP/R045496/1, Low Temperature Heat Recovery and Distribution Network Technologies (LoT-NET). Further capital investment support was provided by the Energy Research Accelerator funded by InnovateUK.

Supplementary materials

Supplementary material associated with this article can be found, in the online version, at doi:10.1016/j.ijrefrig.2022.01.032.

Appendix A

Results from varying the number of nodes, done using the shell manganese chloride test to confirm the number of nodes within the finite difference model

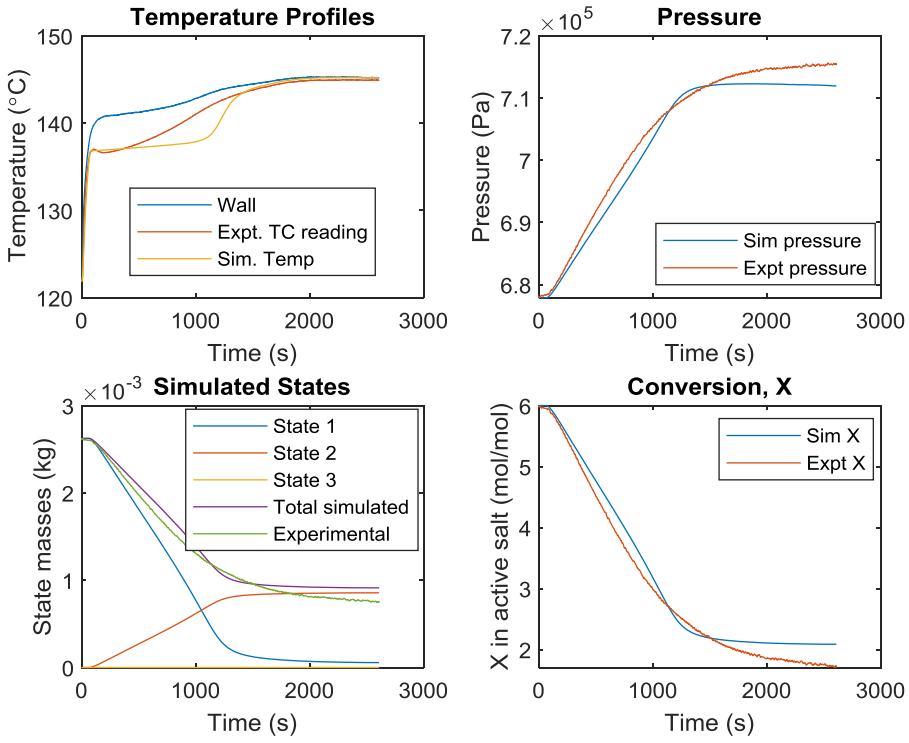

Fig. A1. Shell side result with a 2-node simulation.

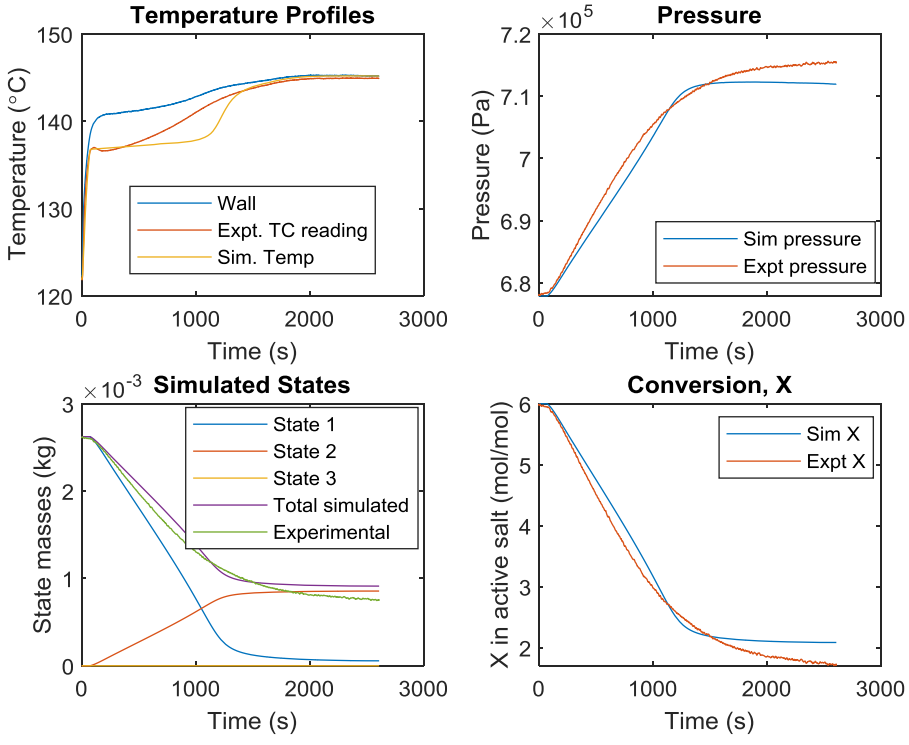

Fig. A2. Shell side with 3 node simulation

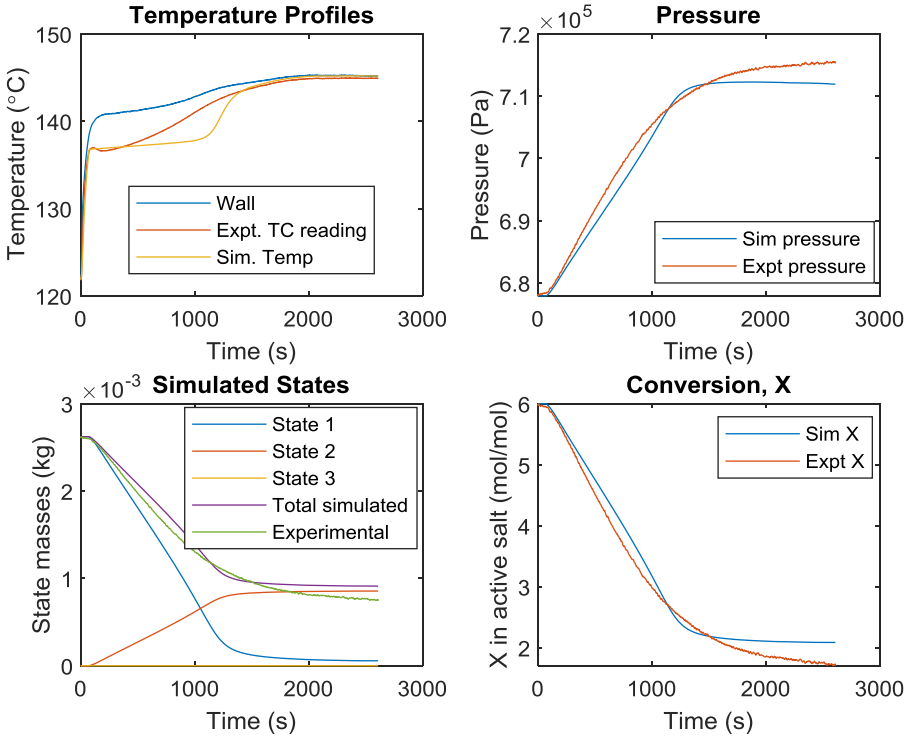

Fig. A3. Shell side result with 4 node simulation

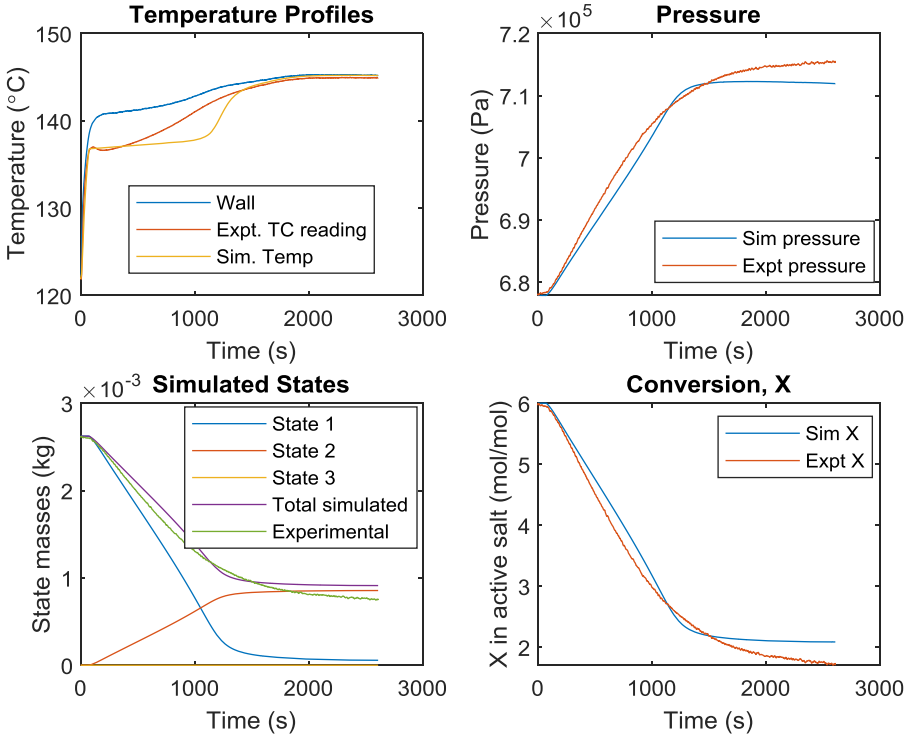

Fig. A4. Shell side result with 5 node simulation

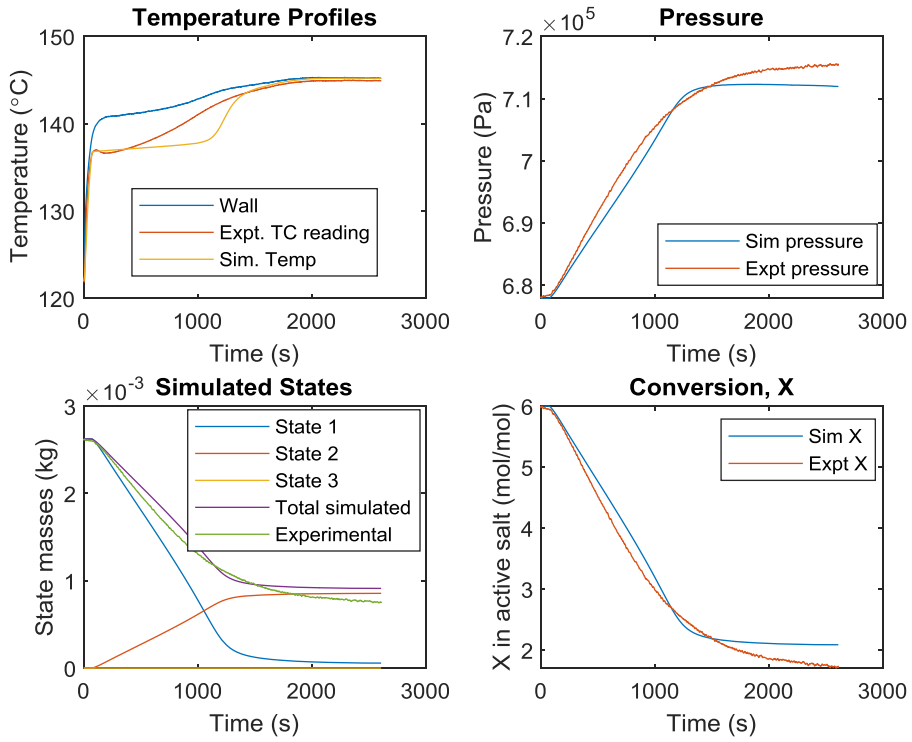

Fig. A5. Shell side result with 10 node simulation

Appendix B

Initial shell side test result with thermoplastic in the void

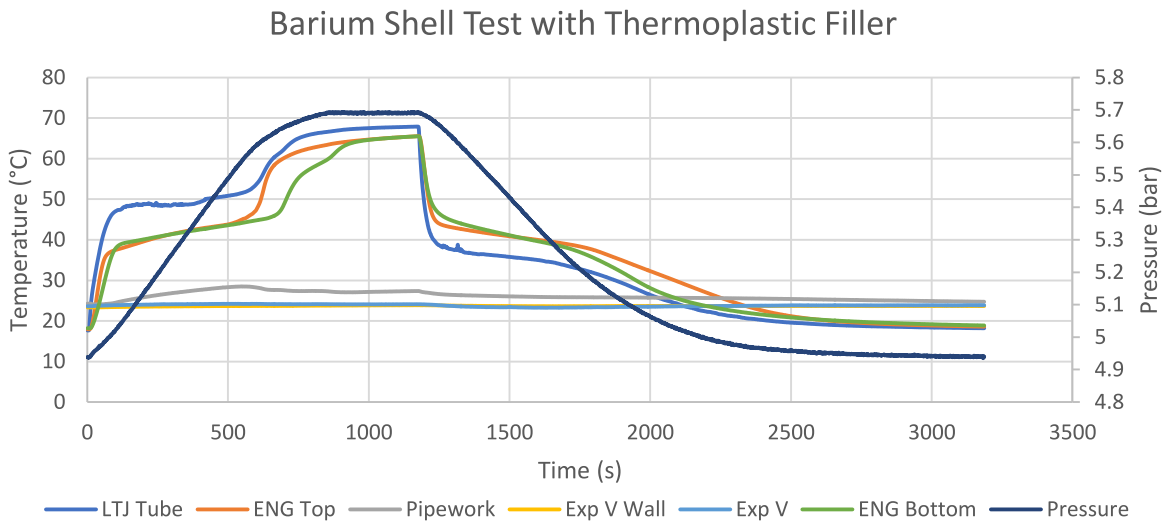

Fig. B1. Shell side tests with thermoplastic PEEK filling the void volume, Initial shell results with PEEK show major lagging in the thermocouple readings and an inability to reach the oil temperature at the end of the reaction, other temperature results monitored are shown in the diagram.

Appendix C

Different barium test results for test c.

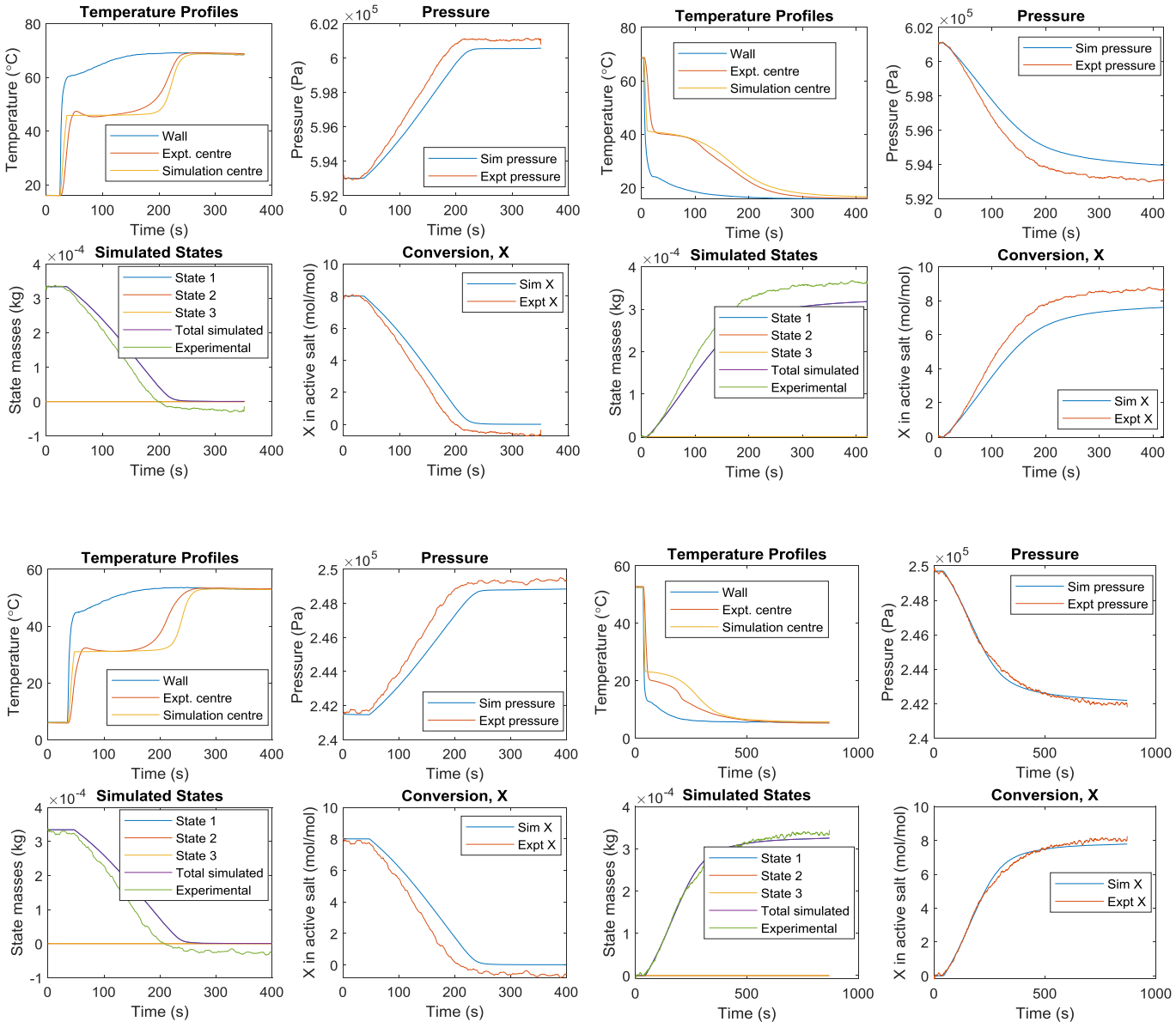

Fig. C1. Different simulation results for test c (table 1) showing good fit.

Appendix D. Simulations results of values from table.

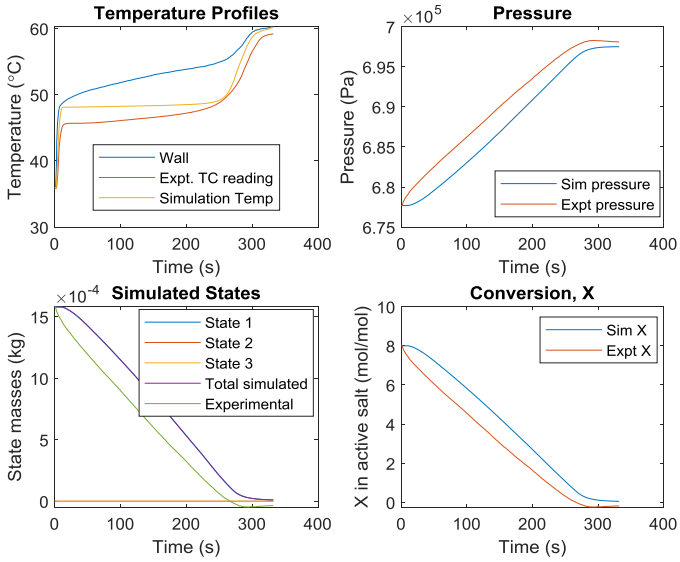

Fig. D1. Simulation result for test e desorption (table 1).

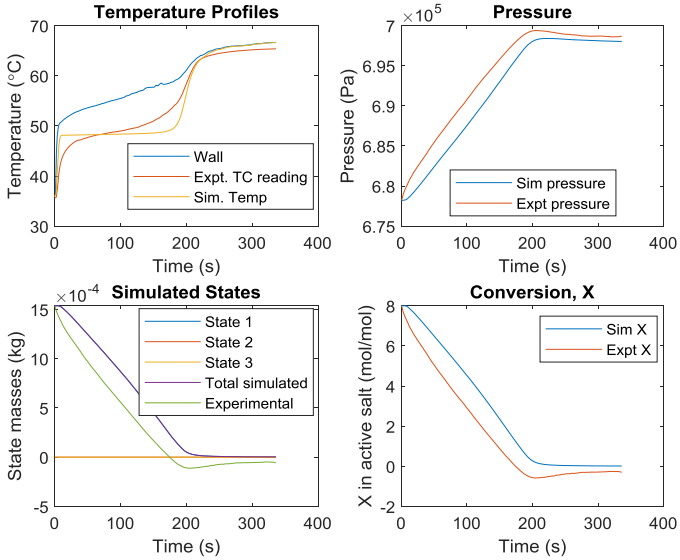

Fig. D2. Simulation for test f desorption (table 1). The heat transfer fluid was water in this case.

Appendix E

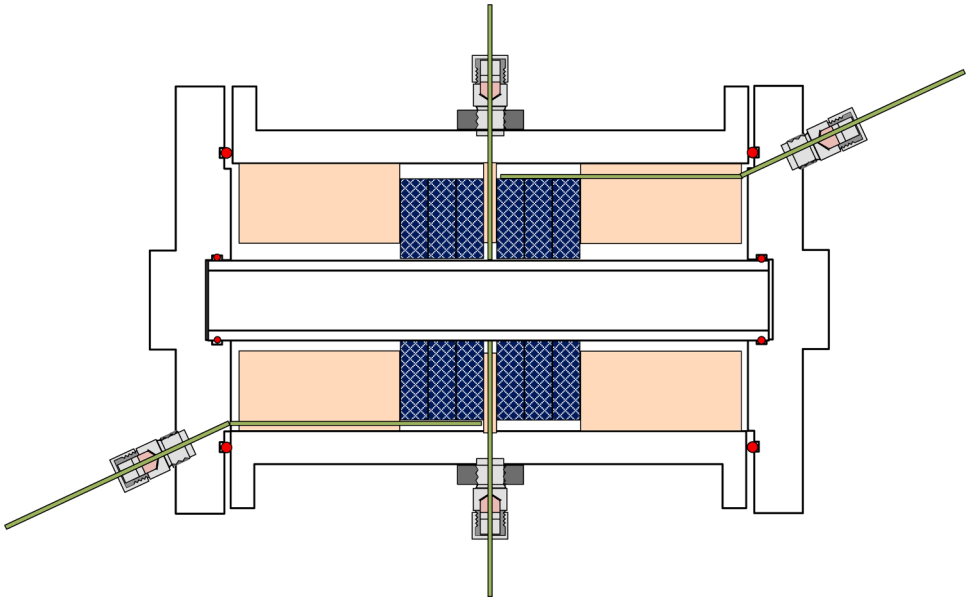

Fig. E1. First shell side design, the length of the reactor was also reduced as it was unnecessarily long and this made it harder to align thermocouples.

References

An, G., Li, Y., Wang, L., Gao, J., 2020a. Wide applicability of analogical models coupled with hysteresis effect for halide/ammonia working pairs. Chemical Engineering Journal 394, 125020.

An, G.L., Wang, L.W., Gao, J., 2019. Two-stage cascading desorption cycle for sorption thermal energy storage. Energy 174, 1091–1099.

An, G.L., Wang, L.W., Zhang, Y.H., 2020b. Overall evaluation of single- and multi-halide composites for multi-mode thermal-energy storage. Energy 212, 118756.

Aristov, Y.I., Dawoud, B., Glaznev, I.S., Elyas, A., 2008. A new methodology of studying the dynamics of water sorption/desorption under real operating conditions of adsorption heat pumps: Experiment. International Journal of Heat and Mass Transfer 51, 4966–4972.

Atkinson, G.H., Hinmers, S., Critoph, R.E., van der Pal, M., 2021. Ammonium Chloride (NH4Cl)—Ammonia (NH3): Sorption Characteristics for Heat Pump Applications. Energies 14.

Bao, H.S., Wang, R.Z., Wang, L.W., 2011. A resorption refrigerator driven by low grade thermal energy. Energy Conversion and Management 52, 2339–2344.

Faraday, M., 1823. On the Condensation of Several Gases into Liquids. Philosophical Transactions of the Royal Society of London 113, 189–198.

Fujioka, K., Kato, S.-i., Fujiki, S., Hirata, Y., 1996. Variations of Molar Volume and Heat Capacity of Reactive Solids of CaCl2 Used for Chemical Heat Pumps. JOURNAL OF CHEMICAL ENGINEERING OF JAPAN 29, 858–864.

Gluesenkamp, K.R., Frazzica, A., Velte, A., Metcalf, S., Yang, Z., Rouhani, M., Blackman, C., Qu, M., Laurenz, E., Rivero-Pacho, A., Hinmers, S., Critoph, R., Bahrami, M., Füldner, G., Hallin, I., 2020. Experimentally Measured Thermal Masses of Adsorption Heat Exchangers. Energies 13, 1150.

Goetz, V., Elie, F., Spinner, B., 1993. The structure and performance of single effect solid-gas chemical heat pumps. Heat Recovery Systems and CHP 13, 79–96.

Goetz, V., Spinner, B., Lépinasse, E., 1997. A solid-gas thermochemical cooling system using BaCl2 and NiCl2. Energy 22, 49–58.

Hinmers, S., Critoph, R.E., 2019. Modelling the Ammoniation of Barium Chloride for Chemical Heat Transformations. Energies 12, 4404.

Hirata, Y., Fujioka, K., 2003. Thermophysical properties and heat transfer characteristics of CaCl2 heat pump reactor associated with structural change of reactive salts, V Minsk international seminar "Heat pipes, heat pumps, refrigerators.

Jegede, O., 2017. Concept Design of a Thermo-Chemical Heat Pump Using Calcium Chloride-Ammonia and Magnesium Chloride-Ammonia Working Pairs. Dept of Engineering. University of Warwick, Coventry.

Lebrun, M., 1990. Simulation for the development of solid—gas chemical heat pump pilot plants Part II. simulation and optimization of Discontinuous and pseudo-continuous operating cycles. Chemical Engineering and Processing: Process Intensification 28, 67–77.

Lebrun, M., Spinner, B., 1990a. Models of heat and mass transfers in solid—gas reactors used as chemical heat pumps. Chemical Engineering Science 45, 1743–1753.

Lebrun, M., Spinner, B., 1990b. Simulation for the development of solid—gas chemical heat pump pilot plants Part I. simulation and dimensioning. Chemical Engineering and Processing: Process Intensification 28, 55–66.

Lépinasse, E., Goetz, V., Crosat, G., 1994. Modelling and experimental investigation of a new type of thermochemical transformer based on the coupling of two solid-gas reactions. Chemical Engineering and Processing: Process Intensification 33, 125–134.

Lépinasse, E., Marion, M., Goetz, V., 2001. Cooling storage with a resorption process. Application to a box temperature control. Applied Thermal Engineering 21, 1251–1263.

Li, T.X., Wang, R.Z., Kiplagat, J.K., Chen, H., 2010. Experimental study and comparison of thermochemical resorption refrigeration cycle and adsorption refrigeration cycle. Chemical Engineering Science 65, 4222–4230.

Ling-Chin, J., Bao, H., Ma, Z., Taylor, W., Roskilly, T., 2019. State-of-the-Art Technologies on Low-Grade Heat Recovery and Utilization in Industry.

Lu, H.-B., Mazet, N., Spinner, B., 1996. Modelling of gas-solid reaction—Coupling of heat and mass transfer with chemical reaction. Chemical Engineering Science 51, 3829–3845.

Mazet, N., Amouroux, M., 1991. Analysis of Heat Transfer in a Non-isothermal Solid-Gas Reacting Medium. Chemical Engineering Communications 99, 175–200.

Mazet, N., Amouroux, M., Spinner, B., 1991. Analysis and Experimental Study of the Transformation of Non-isothermal Solid-Gas Reacting Medium. Chemical Engineering Communications 99, 155–174.

Mazet, N., Spinner, B., 1994. Analyses of irreversibilities and research and development on solid-gas reaction thermochemical transformers. International Journal of Refrigeration 17, 329–337.

Moundanga-Iniamy, M., Touzain, P., 1992. The Reaction between Ammonia and Magnesium Chloride Graphite Intercalation Compounds. MSF Materials Science Forum 91-93, 823–828.

Neveu, P., Castaing, J., 1993. Solid-gas chemical heat pumps: Field of application and performance of the internal heat of reaction recovery process. Heat Recovery Systems and CHP 13, 233–251.

SGL Carbon, 2020. ECOPHIT L and LN. SGL Carbon SE. Available at: https://www.sglcarbon.com/en/markets-solutions/material/ecophit-graphite-lightweight-construction-panels/ (Accessed: 24 January 2022).

Sharonov, V.E., Aristov, Y.I., 2005. Ammonia adsorption by MgCl2, CaCl2 and BaCl2 confined to porous alumina: the fixed bed adsorber. Reaction Kinetics and Catalysis Letters 85, 183–188.

Spinner, B., 1988. Pompes à chaleur basées sur la réaction renversable entre un gaz et un solide on un liquide ou une solution saturée. Récents Progrés en Génie des Procédés 2, 222.

Trudel, J., Hosatte, S., Ternan, M., 1999. Solid–gas equilibrium in chemical heat pumps: the NH3–CoCl2 system. Applied Thermal Engineering 19, 495–511.

van der Pal, M., Critoph, R.E., 2017. Performance of CaCl2-reactor for application in ammonia-salt based thermal transformers. Applied Thermal Engineering 126, 518–524.

Vasiliev, L.L., Mishkinis, D.A., Antukh, A.A., Kulakov, A.G., Vasiliev, L.L., 2004. Resorption heat pump. Applied Thermal Engineering 24, 1893–1903.

Veselovskaya, J.V., Tokarev, M.M., 2011. Novel ammonia sorbents "porous matrix modified by active salt" for adsorptive heat transformation: 4. Dynamics of quasi-

isobaric ammonia sorption and desorption on BaCl2/vermiculite. Applied Thermal Engineering 31, 566–572.
Wang, C., Zhang, P., Wang, R.Z., 2010. Performance of solid–gas reaction heat transformer system with gas valve control. Chemical Engineering Science 65, 2910–2920.
Wu, S., Li, T.X., Yan, T., Wang, R.Z., 2019. Advanced thermochemical resorption heat transformer for high-efficiency energy storage and heat transformation. Energy 175, 1222–1233.
Xu, J., Oliveira, R.G., Wang, R.Z., 2011. Resorption system with simultaneous heat and cold production. International Journal of Refrigeration 34, 1262–1267.
Yang, Z., Qu, M., Gluesenkamp, K.R., 2020. Ammonia-based chemisorption heat pumps for cold-climate heating applications: A comprehensive review. Applied Thermal Engineering 179, 115674.
Yuan, Y., Bao, H., Ma, Z., Lu, Y., Roskilly, A.P., 2019. Investigation of equilibrium and dynamic performance of SrCl2-expanded graphite composite in chemisorption refrigeration system. Applied Thermal Engineering 147, 52–60.
Zhong, Y., Critoph, R.E., Thorpe, R.N., Tamainot-Telto, Z., 2009. Dynamics of BaCl2–NH3 adsorption pair. Applied Thermal Engineering 29, 1180–1186.
Zhong, Y., Critoph, R.E., Thorpe, R.N., Tamainot-Telto, Z., Aristov, Y.I., 2007. Isothermal sorption characteristics of the BaCl2–NH3 pair in a vermiculite host matrix. Applied Thermal Engineering 27, 2455–2462.
Zhou, Z.S., Wang, L.W., Jiang, L., Gao, P., Wang, R.Z., 2016. Non-equilibrium sorption performances for composite sorbents of chlorides–ammonia working pairs for refrigeration. International Journal of Refrigeration 65, 60–68.